ORIGINAL RESEARCH ARTICLE

The Depositional Record

*A journal of the International Association of Sedimentologists*

Open Access

IAS    WILEY

# Overprinted allocyclic processes by tidal resonance in an epicontinental basin: The Upper Jurassic Curtis Formation, east-central Utah, USA

Valentin Zuchuat[1] [iD]    |    Arve R. N. Sleveland[1]    |    Ross P. Pettigrew[2]    |    Thomas J. H. Dodd[2,3] [iD]    |    Stuart M. Clarke[2]    |    Ole Rabbel[1]    |    Alvar Braathen[1]    |    Ivar Midtkandal[1]

[1]Tectonostratigraphic Research Group, University of Oslo, Oslo, Norway

[2]Basin Dynamics Research Group, Keele University, Keele, Staffordshire, UK

[3]British Geological Survey, The Lyell Centre, Edinburgh, UK

**Correspondence**
Valentin Zuchuat, Tectonostratigraphic Research Group, University of Oslo, Oslo, Norway.
Email: valentin.zuchuat@geo.uio.no

**Funding information**
Norges Forskningsråd, Grant/Award Number: 244049

## Abstract

Modern, tide-dominated and tide-influenced coastlines are characterized by a range of environments, including deltas, estuaries and lagoons. However, some tide-dominated basins and related sedimentary units in the rock record, such as the semi-enclosed, shallow, Utah–Idaho Trough foreland basin of the Jurassic Curtis Sea, do not correspond to any of these modern systems. Persistent aridity caused the characteristic severe starvation of perennial fluvial input throughout this basin, in which the informal lower, middle and upper Curtis, as well as the underlying Entrada Sandstone, and the overlying Summerville Formation were deposited. Wave energy was efficiently dissipated by the shallow basin's elongated morphology (approximately 800 × 150 km), as its semi-enclosed morphology further protected the system from significant wave impact. Consequently, the semi-enclosed, shallow-marine system was dominated by amplified tidal forces, resulting in a complex distribution of heterolithic deposits. Allocyclic forcing strongly impacted upon the system's intrinsic autocyclic processes as the lower Curtis was deposited. Short-lived relative sea-level variations, along with uplift and deformation episodes, resulted in the accumulation of three parasequences, each separated by traceable flooding and ravinement surfaces. The subsequent transgression, which defines the base of the middle Curtis, allowed for the shallow-marine part of the system to enter into tidal resonance as a consequence of the flooded basin reaching the optimal configuration of approximately 800 km in length, corresponding to an odd multiple of the quarter of the tidal wavelength given an average minimum water depth of 20–25 m. This resonant system overprinted the effects of allocyclic forcing and related traceable stratigraphic surfaces. However, the contemporaneous and neighbouring coastal dune field sedimentary rocks of the Moab Member of the Curtis Formation, characterized by five stacked aeolian sequences, as well as the supratidal deposits of the Summerville Formation, lingered to record allocyclic signals, as the Curtis Sea regressed. This study shows that a tide-dominated basin can enter into tidal resonance as it reaches

its optimal morphological configuration, leading to the overprinting of otherwise dominant allocyclic processes by autocyclic behaviour. It is only by considering the sedimentological relationships of neighbouring and contemporaneous depositional systems that a full understanding of the dynamic stratigraphic history of a basin alternatively dominated by autocyclic and allocyclic processes can be achieved.

# 1 | INTRODUCTION

Oceanic tides and their spatio-temporal variability are complex and dynamic phenomena (Kvale, 2012). The environments they act upon have raised people's interest as early as the first century AD, when Pliny the Elder described areas "invaded twice each day and night by the overflowing waves of the ocean", leaving one to wonder if they "are to be looked upon as belonging to the land, or whether as forming portion of the sea?" (translation from Bostock & Riley, 1855).

Sedimentary successions deposited within tide-dominated basins are characterized by a three-dimensional (3D), complex and potentially cyclic assemblage of heterolithic lithologies, the distribution of which depends on a fine balance between (a) basin configuration and the dispersal of basinal hydrodynamic forces, (b) autogenic basin processes, such as the avulsion of tidal channels, and (c) sediment input (Kvale, 2012; Wang, 2012, and references therein). Spatio-temporal variations of tidal currents, which variably influence the system's erosion–transport–deposition chain, further complicate the arrangement of these deposits. (Baas, Best, & Peakall, 2016; Kvale, 2012; Wang, 2012). These intrinsic and interacting processes, and their associated patterns of sedimentation, are ultimately governed by allocyclicly driven phenomena (Osleger, 1991), such as variations in relative sea level and changes in available accommodation, and by the rate and frequency at which they occur (Strasser, Pittet, Hillgärtner, & Pasquier, 1999). To complicate further the interpretation of the deposits of a tide-dominated basin, sediment deposition typically takes place upon a low-gradient slope and facies belts are shifted over large horizontal distances by comparatively small variations in water depth (Midtkandal & Nystuen, 2009; Zuchuat et al., 2018). In addition, modern-day, semi-enclosed basins, such as the Gulf of California, the Adriatic Sea, the Persian Gulf, or the Bay of Fundy, demonstrate that basin geometry can further amplify tidal forces, allowing the system to enter a tidal resonant stage if the length of the basin approximates to an odd multiple of a quarter of the tidal wavelength (Longhitano, Mellere, Steel, & Ainsworth, 2012; Martinius & Gowland, 2011; Reynaud & Dalrymple, 2012;

Roos & Schuttelaars, 2011; Shaw, Todd, & Li, 2014; Sztanó & de Boer, 1995). A consequence of this is augmented tidal ranges and stronger tidal currents closer to the shoreline than in open water (Godin, 1993; Longhitano et al., 2012; Martinius & Gowland, 2011; Reynaud & Dalrymple, 2012; Roos & Schuttelaars, 2011; Shaw et al., 2014; Sztanó & de Boer, 1995; Yoshida, Steel, & Dalrymple, 2007).

The impact of such autocyclic processes has been detected in sediments deposited in transgressive settings, as the system's resonance typically increases with a relative sea-level rise (Longhitano et al., 2012; Martinius & Gowland, 2011; Reynaud & Dalrymple, 2012; Sztanó & de Boer, 1995; references therein). However, the time required to trigger or abandon a tidal resonance is geologically instantaneous, and the time interval encapsulated by the deposited sediments can be short, compound, and spatially variable, as different parts of the basin become resonant at different times (Reynaud & Dalrymple, 2012).

Despite a complicated and spatio-temporally compartmentalized sedimentary architecture, tidally dominated sedimentary successions typically host reservoir grade sandstone bodies that are often laterally and vertically sealed by finer grained, low porosity and low permeability sediments. Consequently, these sedimentary systems have significant potential in containing reservoir targets for the hydrocarbon exploration industry, aquifer appraisal, and $CO_2$ sequestration projects (Halland et al., 2014; Martinius et al., 2005).

Notwithstanding the inherent complexities of sediment character and distribution, most shallow-water, tide-dominated, coastal depositional systems can be classified as (a) transgressive, upward-fining estuaries, (b) (semi-) protected lagoons, (c) prograding, tide-dominated deltas, or (d) open-coast tidal flat (Figure 1; Boyd, Dalrymple, & Zaitlin, 1992; Dalrymple, Zaitlin, & Boyd, 1992; Harris et al., 2002; Fan, 2012). However, not every sedimentary succession that displays evidence of tidal reworking corresponds to one of these four end members. Broad, shallow epicontinental basins (Tape, Cowan, & Runkel, 2003; Zuchuat et al., 2018), and fluvially starved macro-embayments (Zuchuat et al., 2018) may display strong
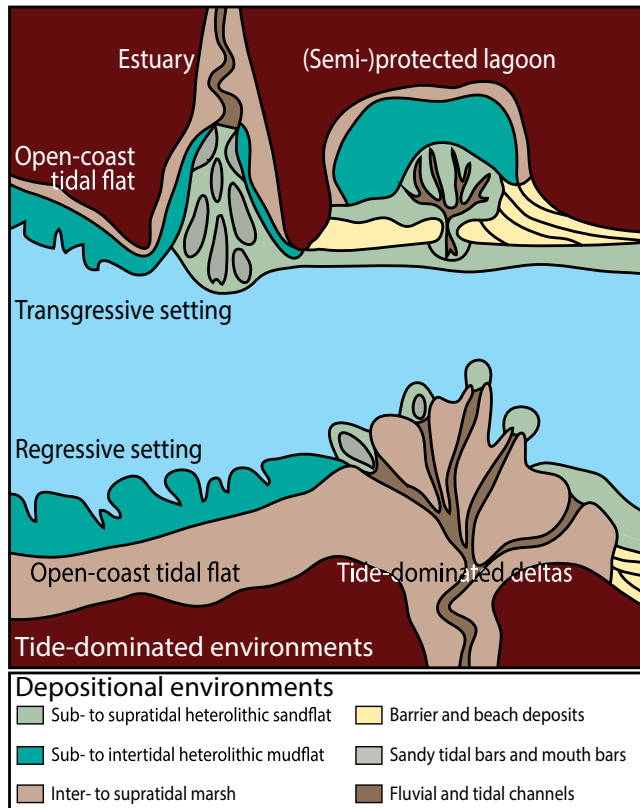
**FIGURE 1** Modern day, tide-dominated coastline environments (modified from Boyd et al., 1992; Harris et al., 2002; Fan, 2012)

evidence for tidal reworking of sediments within them, but a lack of modern day equivalents hampers interpretation of the sedimentary record, especially when 3D continuous exposure is unavailable.

The continuous and 3D exposure of the middle to upper Jurassic succession of east-central Utah (Figure 2) allows detailed investigations of a shallow-marine to marginal aeolian environment that evolves into a semi-enclosed, fluvially starved and tidally influenced, epeiric setting through time.

This study provides a detailed analysis of the Middle Jurassic Entrada Sandstone and the Upper Jurassic Curtis and Summerville formations (Wilcox & Currie, 2008) within the context of Zuchuat et al.'s (2018) lower, middle and upper Curtis lithostratigraphic framework, and develops that framework further to reconstruct the kinematic history of the transition from an aeolian to a shallow-marine basin. The assessment of the Moab Member of the Curtis Formation (Caputo & Pryor, 1991; Doelling, 2001; Peterson, 1994; Zuchuat et al., 2018) offers further insights into the behaviour of neighbouring aeolian deposits and their relationships to the contemporaneous shallow-marine and paralic realm. The work presented in this article identifies key sequence stratigraphic surfaces, such as flooding surfaces, that are the result of high-frequency systemic responses to varying climate conditions and changes in relative sea level (Alberti, Fürsich, 2012; Boulila et al., 2010, 2011; Pellenard et al.,

2014; Strasser, Vedrine, & Stienne, 2012), as well as basinal reconfiguration during the Oxfordian Age. Identified and traceable stratigraphic surfaces are probably a consequence of allocyclic forcing, but evidence for this within part of the succession is overprinted periodically by the sedimentary response to autocyclic processes, most notably when the tide-dominated embayment enters a resonant stage. Consequently, the study illustrates the value in identifying key sequence stratigraphic surfaces for correlating highly heterolithic, tidally influenced sedimentary packages.

Through an assessment of the sedimentology, and correlation of the stratigraphic relationships between the Entrada Sandstone, the Curtis Formation and the Summerville Formation in the vicinity of the San Rafael Swell area of south-central Utah (Figure 2), this study has the following aims: (a) to demonstrate that dominant allocyclic signatures in the sediments can be overprinted and obliterated by those of autogenic processes and (b) to understand and interpret shallow-marine systems, in settings where overprint occurs, through a knowledge of neighbouring and contemporaneous systems in order to fully assess the basin's history.

## 2 | GEOLOGICAL SETTING

### 2.1 | Tectonic setting

Four major tectonic events have impacted on Utah's geological development since the early Mesozoic, and the rise of the North American Cordillera (Anderson, 2015; Hintze & Kowallis, 2009; Thorman, 2011; Yonkee & Weil, 2015; and references therein): (a) the Nevadan Orogeny (Middle Jurassic–Lower Cretaceous), whose granitic intrusions can be observed at today's Utah–Nevada border; (b) the Elko Orogeny (Middle Jurassic), characterized by alternating episodes of tectonic contraction and extension, accompanied by the development of SSW-NNE-striking, stacked foreland basin development; (c) the Sevier Orogeny (Lower Cretaceous to Palaeogene), featuring thin and thick-skinned, east-directed fold-thrust belt structures in Idaho–Utah–Wyoming, and (d) the Laramide Orogeny (Upper Cretaceous to Palaeogene), associated with the development of basement-rooted monoclines, such as the San Rafael Swell (Bump & Davis, 2003). The stratigraphy of central-eastern Utah was also affected by diapirism and remobilization of the Paradox Basin evaporitic strata (Trudgill, 2011), as well as by the Colorado Plateau uplift and its sub-regional to regional extensional episodes (Levander et al., 2011; Murray, Reiners, & Thomson, 2016). The igneous intrusive complexes of the Abajo, Henry and La Sal mountains (Upper Oligocene) also impacted on the sedimentary strata in central-eastern Utah (Nelson, 1997; Sullivan, Kowallis, & Mehnert, 1991). The Upper Callovian to Lower Oxfordian Entrada–Curtis–Summerville lithostratigraphic sub-divisions were deposited within the Utah–Idaho

Trough, a SSW–NNE-oriented retroarc foreland basin at the foot of the Elko Highlands (Thorman, 2011), which the northerly located Sundance Sea flooded several times during its history (Hintze & Kowallis, 2009).

## 2.2 | Stratigraphy

The Middle Jurassic coastal to shallow-marine Temple Cap Formation, the shallow to marginal-marine Carmel Formation, the continental Entrada Sandstone of south-eastern Utah,

and the overlying Upper Jurassic Curtis and Summerville formations comprise the San Rafael Group of the Colorado Plateau (Figure 2; Anderson & Lucas, 1994; Doelling, 2001; Doelling, Sprinkel, Kowallis, & Kuehne, 2013; Gilluly & Reeside, 1928; Peterson & Pipiringos, 1979; Pipiringos & O'Sullivan, 1978; Sprinkel, Doelling, Kowallis, Waanders, & Kuehne, 2011; Sprinkel, Kowallis, & Jensen, 2011). These successions represent five upward-thinning, transgressive-regressive (TR) sequences with an eastward and southward-wedging geometry that is a consequence of deposition within
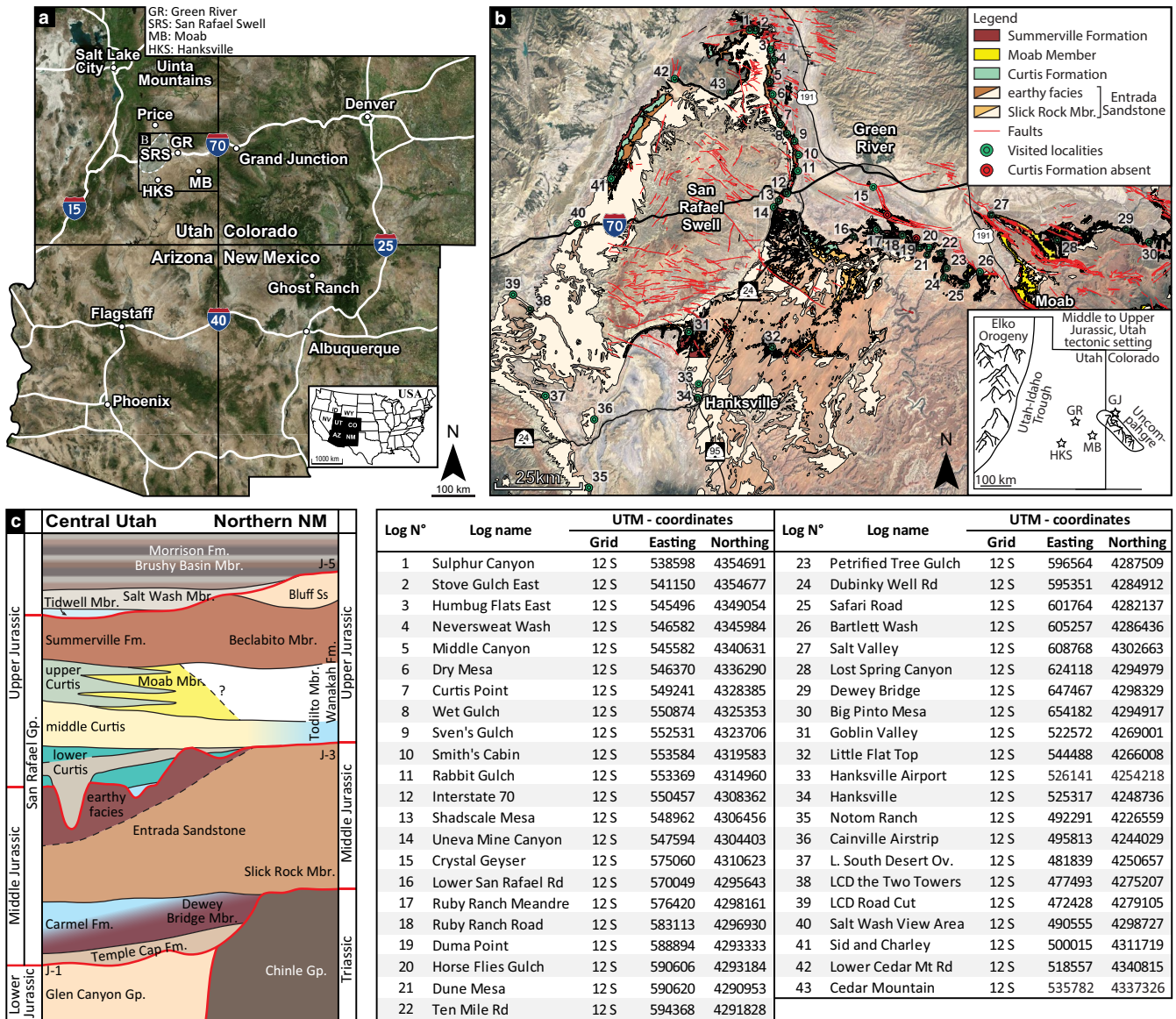


| Log N° | Log name | UTM - coordinates | | | Log N° | Log name | UTM - coordinates | | |
|---|---|---|---|---|---|---|---|---|---|
| | | Grid | Easting | Northing | | | Grid | Easting | Northing |
| 1 | Sulphur Canyon | 12 S | 538598 | 4354691 | 23 | Petrified Tree Gulch | 12 S | 596564 | 4287509 |
| 2 | Stove Gulch East | 12 S | 541150 | 4354677 | 24 | Dubinky Well Rd | 12 S | 595351 | 4284912 |
| 3 | Humbug Flats East | 12 S | 545496 | 4349054 | 25 | Safari Road | 12 S | 601764 | 4282137 |
| 4 | Neversweat Wash | 12 S | 546582 | 4345984 | 26 | Bartlett Wash | 12 S | 605257 | 4286436 |
| 5 | Middle Canyon | 12 S | 545582 | 4340631 | 27 | Salt Valley | 12 S | 608768 | 4302663 |
| 6 | Dry Mesa | 12 S | 546370 | 4336290 | 28 | Lost Spring Canyon | 12 S | 624118 | 4294979 |
| 7 | Curtis Point | 12 S | 549241 | 4328385 | 29 | Dewey Bridge | 12 S | 647467 | 4298329 |
| 8 | Wet Gulch | 12 S | 550874 | 4325353 | 30 | Big Pinto Mesa | 12 S | 654182 | 4294917 |
| 9 | Sven's Gulch | 12 S | 552531 | 4323706 | 31 | Goblin Valley | 12 S | 522572 | 4269001 |
| 10 | Smith's Cabin | 12 S | 553584 | 4319583 | 32 | Little Flat Top | 12 S | 544488 | 4266008 |
| 11 | Rabbit Gulch | 12 S | 553369 | 4314960 | 33 | Hanksville Airport | 12 S | 526141 | 4254218 |
| 12 | Interstate 70 | 12 S | 550457 | 4308362 | 34 | Hanksville | 12 S | 525317 | 4248736 |
| 13 | Shadscale Mesa | 12 S | 548962 | 4306456 | 35 | Notom Ranch | 12 S | 492291 | 4226559 |
| 14 | Uneva Mine Canyon | 12 S | 547594 | 4304403 | 36 | Cainville Airstrip | 12 S | 495813 | 4244029 |
| 15 | Crystal Geyser | 12 S | 575060 | 4310623 | 37 | L. South Desert Ov. | 12 S | 481839 | 4250657 |
| 16 | Lower San Rafael Rd | 12 S | 570049 | 4295643 | 38 | LCD the Two Towers | 12 S | 477493 | 4275207 |
| 17 | Ruby Ranch Meandre | 12 S | 576420 | 4298161 | 39 | LCD Road Cut | 12 S | 472428 | 4279105 |
| 18 | Ruby Ranch Road | 12 S | 583113 | 4296930 | 40 | Salt Wash View Area | 12 S | 490555 | 4298727 |
| 19 | Duma Point | 12 S | 588894 | 4293333 | 41 | Sid and Charley | 12 S | 500015 | 4311719 |
| 20 | Horse Flies Gulch | 12 S | 590606 | 4293184 | 42 | Lower Cedar Mt Rd | 12 S | 518557 | 4340815 |
| 21 | Dune Mesa | 12 S | 590620 | 4290953 | 43 | Cedar Mountain | 12 S | 535782 | 4337326 |
| 22 | Ten Mile Rd | 12 S | 594368 | 4291828 | | | | | |

**FIGURE 2** (a, b) Maps of the study area. Green dots represent visited localities where the Curtis Formation crops out, while the red dots illustrate its absence. Each code number on the map refers to a specific locality in the attached table (Geological units after Hintze, 1980; Witkind, 1988; Doelling, 2001; Doelling et al., 2013, 2015; Sprinkel, et al., 2011; a, b; Tectonic setting after Heyman, 1983; Thorman, 2011; satellite images © Google Earth). GJ, Grand Junction; GR, Green River; HKS, Hanksville; MB, Moab; SRS, San Rafael Swell. (c) Schematic lithostratigraphic column showing a correlation between the San Rafael Swell area, east-central Utah, and Ghost Ranch, in northern New Mexico (Doelling, 2001; Doelling et al., 2015; Kocurek et al., 2018; Zuchuat et al., 2018;). Note that the contemporaneous character between the Entrada Sandstone and the lower Curtis, as well as between the middle Curtis, upper Curtis, Moab Member, and Summerville Formation is not shown in this lithostratigraphic display

the Utah–Idaho Trough (Figure 2b; Anderson & Lucas, 1994; Bjerrum & Dorsey, 1995; Brenner & Peterson, 1994; Peterson, 1994; Thorman, 2011).

As the Jurassic shallow and epeiric Sundance Sea regressed northward during the Callovian Age and warm arid conditions prevailed, sediments of the shallow to marginal-marine Carmel Formation (Figure 2c) were overlain conformably by those of the marginal-marine to continental, rusty-red to light-orange, aeolian Entrada Sandstone (Figure 2c; Gilluly & Reeside, 1928; Hintze & Kowallis, 2009; Peterson, 1994). Recent $^{40}Ar/^{39}Ar$ age determinations of tephra layers within the uppermost strata of the Entrada Sandstone in southern Utah provide an Oxfordian depositional date of $160.8 \pm 0.4$ Ma (Dossett, 2014). In east-central Utah, the Entrada Sandstone is divided typically into (a) the Slick Rock Member that comprises aeolian dune and interdune sediments, and (b) the overlying and partially contemporary informal unit of the 'earthy facies' (Imlay, 1952), characterized by repeated, yet extraneously vegetated, mottled loess strata, interbedded with marginal-marine sabkha-like deposits (Doelling et al., 2015; Witkind, 1988; and references therein). The Entrada Sandstone thickens westwards, in the direction of the Utah–Idaho Trough, and northwards, towards the Uinta Mountains (Figure 2; Carr-Crabaugh & Kocurek, 1998; Crabaugh & Kocurek, 1993; Doelling et al., 2015; Kocurek & Havholm, 1993; Mountney, 2012; Witkind, 1988). The earthy facies thins out to the south and east of the study area (Figure 2b), where the sediments of the Curtis Formation directly overlie the Slick Rock Member. Recycled fluvial sediments are the main constituents of the Entrada Sandstone, indicative of a drainage system that originated from basement rocks of today's Appalachian Mountains (Dickinson & Gehrels, 2009, 2010). Four 'construction–destruction' sequences (sensu Mountney, 2006), related to regional base-level oscillations, are recognized within this coastal aeolian system (Carr-Crabaugh & Kocurek, 1998; Kocurek, 2003; Kocurek & Lancaster, 1999; Mountney, 2012), and the Entrada Sandstone is capped at its top by the regional, polygenetic and heterochronous J-3 Unconformity (Zuchuat et al., 2018, in press), first defined by Pipiringos and O'Sullivan (1978). The unconformity displays relief with an amplitude ranging from 0.1 to 23 m, and a wavelength varying from the decimetre to the hectometre scale (Zuchuat et al., in press). Relief was generated by both erosion-related and deformational processes, and surface types include flat angular unconformities, paraconformities, steep tidal incisions, sinuous undulations, irregular tidal ravinement surfaces, circular collapse structures, sedimentary loading, and hydroplastic sagging (Zuchuat et al., in press).

The Entrada Sandstone is overlain by the lower Oxfordian Curtis Formation, originally defined by Gilluly and Reeside (1928) from exposures along the northeast margin of the San Rafael Swell (Figure 2). The Curtis sediments comprise complexly arranged, shallow-marine packages of tidally influenced heterolithic strata (Caputo & Pryor, 1991; Kreisa & Moiola, 1986; Ogg, Ogg, & Gradstein, 2016; Wilcox & Currie, 2008; Zuchuat et al., 2018) deposited as the Curtis Sea flooded a gently dipping, shallow, and fluvially starved, epicontinental basin that developed as the rate of accommodation development diminished at end of the Callovian Age (Thorman, 2011; Zuchuat et al., 2018). The underrepresentation of wave-related structures within the Curtis Formation can be attributed to the protected nature of the Curtis Sea, as well as the elongate basin configuration, which facilitated dissipation of wave energy (Yoshida et al., 2007). Sediments of the Curtis Formation have a green to white colouration, which is due to the presence of glauconite and chlorite. The colour strongly contrasts with the underlying rusty-red terrestrial Entrada Sandstone (Caputo & Pryor, 1991; Gilluly & Reeside, 1928; Peterson, 1994).

It is possible to infer the Curtis Sea basin reached approximately 800 km in length (Dickinson & Gehrels, 2003; Peterson, 1994), and at least 150 km in width, based on stratigraphic relationships between the studied Curtis–Summerville interval, and equivalent succession in neighbouring areas: the Curtis–Summerville interval is the lateral equivalent of the Stump Formation further north in the Uinta Mountains area (Figure 2a; Imlay, 1980; Pipiringos & Imlay, 1979; Wilcox & Currie, 2008). It corresponds to the Redwater Shale Member of the Sundance Formation in Wyoming (Imlay, 1947, 1980); and to the Stump Formation in the vicinity of the Wyoming-Idaho border (Imlay, 1980; Mansfield & Roundy, 1916; Pipiringos & Imlay, 1979). As a result, the Curtis Formation is characterized by an east and south-wedging geometry, with a maximum thickness of approximately 80 m at Sven's Gulch (9*), in the San Rafael Swell area (Anderson, 2015; Caputo & Pryor, 1991; Gilluly & Reeside, 1928; Peterson, 1994; Thorman, 2011; see Figure 2 and fig. 3 in Zuchuat et al., 2018). The Curtis Formation is separated into three informal units based upon their outcrop character: the lower, middle, and upper Curtis (Figure 2; Zuchuat et al., 2018). The lower Curtis comprises laterally restricted upper shoreface to beach deposits, grading into thinly bedded, dark green to grey, heterolithic subtidal flat deposits in which gravel-rich, subtidal channels and dunes occur (Zuchuat et al., 2018). The overlying middle Curtis is characterized by a lighter coloured and better sorted sandstone by comparison to the underlying heterolithic lower Curtis (Zuchuat et al., 2018). Its base corresponds to the regional Major Transgressive Surface (MTS), and consists of complex arrangements of subtidal channels, subtidal to intertidal dune and flat deposits (Zuchuat et al., 2018). The dark green, upper Curtis conformably overlies the middle Curtis, and comprises thinly bedded, subtidal to intertidal deposits, which grade into the supratidal deposits of the Summerville Formation (Zuchuat et al., 2018). Towards the Utah–Colorado border (Figure 2), these deposits form lateral and contemporaneous equivalents to

the aeolian deposits that form the Moab Member of the Curtis Formation (Caputo & Pryor, 1991; Doelling, 2001; Peterson, 1994; Zuchuat et al., 2018).

In the study area (Figure 2), the upper Curtis is overlain conformably by dark brown, sabkha deposits of the Summerville Formation (Caputo & Pryor, 1991; Gilluly & Reeside, 1928; Lucas, 2014; Peterson, 1994). However, in what were unflooded neighbouring regions to the east and to the south, the Summerville Formation likely formed as a contemporaneous coastal plain environment (Zuchuat et al., 2018).

In the 'Four Corners' area, where the states of Utah, Colorado, Arizona and New Mexico meet (Figure 2a), the Todilto Member of the Wanakah Formation is the lateral equivalent of the Curtis Formation, whereas the Beclabito Member of the Wanakah Formation corresponds to the Summerville Formation (Figure 2c; Condon & Huffman, 1988; Kocurek et al., 2018; Zuchuat et al., 2018).

The Curtis-Summerville interval corresponds to Peterson's (1994) fifth (TR) cycle within the Jurassic system of the Sundance Sea and the Western Interior Basin (McMullen, Holland, & O'Keefe, 2014; Pipiringos & O'Sullivan, 1978), and likely corresponds to the LZA-2.3 third-order TR-interval of Haq, Hardenbol, and Vail (1987), post-calibration onto Wilcox and Currie's (2008) age and Ogg et al. (2016) timescale.

## 3 | DATA AND METHODS

The data necessary for this study were gathered during three field campaigns between 2015 and 2018. The study area in central-eastern Utah (Figure 2) extends from the Humbug Flats (1–5), north of the San Rafael Swell, southward to Notom Ranch (35), 44 km southwest of Hanksville, and from Last Chance Desert (38 and 39) on the western margin of the San Rafael Swell, eastward to Big Pinto Mesa (30) on the Utah–Colorado border. In order to cover the study area systematically along the exposure of the Entrada–Curtis–Summerville interval, 43 localities were visited (Figure 2). Of these, 41 outcrop sections were measured and a total of 2,291 m were logged across the Entrada–Curtis–Summerville stratigraphic interval. A total of 869 palaeocurrent readings were collected from 3D exposed dunes and ripples. Additional structural information was collected, including the dip and dip direction of sedimentary strata, fractures and faults, as well as the magnitude of fault displacements. Standard techniques in lithofacies analysis and architectural–element analysis (Walker, 1992) were used in order to permit interpretation of depositional settings. To augment the sedimentary detail, 35 m of section covering the Entrada–Curtis–Summerville interval were logged using a hand-held gamma-ray spectrometer in full assay mode at 20 cm intervals. The gamma-ray data allowed for the extraction of thorium and uranium values, which were used to determine the degree of continental involvement or the marine

influences over the paralic deposits (Fertl, Chilingarian, & Yen, 1982). Interpretation of these data must be considered within the context of the sediment calibre: thorium/uranium (Th/U) ratios as a discriminator of marine over continental provenance are reliable in mud-dominated successions (Fertl Chilingarian, & Yen, 1982), yet they remain relevant for coarser-grained sediments as well (Svendsen & Hartley, 2001).

This dataset is complemented by aerial images, photographic material collected at and between the visited localities using standard, handheld cameras and unmanned aerial vehicles. In order to document, illustrate and understand the complex 3D sedimentary architecture of the interval of interest, 3D virtual outcrop models were produced from the collected photogrammetric material (after Westoby, Brasington, Glasser, Hambrey, & Reynolds, 2012). The models were generated using PhotoScan Pro© (Agisoft LLC, St. Petersburg, Russia), before being analysed and interpreted with Lime©, a software developed by the Virtual Outcrop Geology group of both Bergen and Aberdeen universities (Bonaventura et al., 2017; Buckley, Ringdal, Dolva, Naumann, & Kurz, 2017).

Merging sedimentary data with photogrammetric models and structural data sets provided a means of tracing key sequence stratigraphic surfaces, such as subaerial unconformities, transgressive surfaces, regressive surfaces of marine erosion, flooding surfaces and tidal ravinement surfaces (sensu Catuneanu, 2006; Catuneanu et al., 2009) to provide a regional sequence stratigraphic framework and interpretation.

## 4 | RESULTS

The facies (Table 1) and facies associations (FA) schemes (Table 2) which are developed in this work summarize Zuchuat et al.'s (2018) detailed sedimentological assessment of the Curtis Formation and its neighbouring units. Combined with an understanding of the J-3 Unconformity development (described by Zuchuat et al., in press), they are used to decipher the dynamic history of the basin, and to identify depositional environments and their spatiotemporal relationships.

### 4.1 | FA 1 – Coastal wet aeolian deposits

#### 4.1.1 | Description

The Entrada Sandstone at the base of the studied interval comprises two FAs that are broadly comparable to the unit's lithostratigraphic subdivisions. FA 1a consists of mostly cross-stratified aeolian dunes and interdune deposits belonging to the Slick Rock Member of the Entrada Sandstone. FA 1b corresponds to the rusty-red, informal earthy facies of the Entrada Sandstone, and comprises

**TABLE 1**  Facies description for the Entrada Sandstone, Curtis Formation, and Summerville Formation

| Facies | Description | Structures | Grain size | Interpretation | Formation |
|---|---|---|---|---|---|
| A | Cross-stratified sandstone | Unidirectional tangential cross-bedded vf-f grained sandstone, alternating grain flow and grain fall deposits, sharp base, rusty red or white, locally bleached, local occurrence of rhizoliths, varying bedform/bedform sets size, maximum individual dune thickness 15 m. Potential occurrence of counter-ripples at the toe of the foresets | VF – F | Aeolian dune deposits, locally influenced by a dynamic and migrating water table/saturated level | Entrada Ss Moab Mbr |
| B | Plane parallel-laminated to mottled mudstone with localized evaporites | Dark red silty mudstone with pale yellow to white vf-f grained sand lenses, plane parallel-laminated to -stratified or mottled, potential bleached patches around rhizoliths, localized evaporite-rich horizons, maximum individual horizon thickness 1 cm | Si – Cl | Aeolian interdune to coastal plain domain with occasional flooding with development of sabkha-type deposits and/or superficial vegetation | Entrada Ss Summerville Fm. |
| C | Tangential cross-stratified sandstone | Trough cross-stratified vf-m grained sandstone, common rippled reactivation surfaces, potential mud drapes and rip-up mud clasts, eventual desiccation cracks and/or evaporite-rich horizons. Thickness ranging between dm- to m values | VF – M | Tidally influenced migrating 3D-dunes | Entrada Fm. Curtis Fm. Summerville Fm. |
| D | Structureless fluidized sandstone | Deformed to structureless fluidized of green to pink silt- to fine-grained sandstone, local fluid-escape and loading structures still visible, sometimes visually expressed as well rounded sandstone boulders with injected mudstone, maximum boulder Ø 25 cm, maximum bed thickness 2 m | Si-F | Destruction of original sedimentary structures due to fluids flowing through the sandstone bed or through liquefaction of water-saturated horizons | Entrada Ss Curtis Fm. |
| E | Thoroughly bioturbated condensed sandstone | Rusty-red condensed, cemented, fine-grained sandstone, thoroughly bioturbated, maximum thickness 25 cm | F | Sediment starvation in a semi-arid coastal plane setting | Entrada Ss |
| F | Matrix-supported basal conglomerate | Rounded to well-rounded, matrix-supported basal conglomerate, no preferred clast orientation but their long axis tend to be parallel to the bedding plane, matrix consists of f- to m-grained sandstone, maximum clast Ø 8 cm, maximum bed thickness 20 cm | F-Pb | Flash flood deposits | Curtis Fm. ? |
| G | Planar- to low angle cross-stratified sandstone | Plane-parallel- to low angle cross-stratified vf-f grained grey to green to white sandstone, potential herringbone cross-lamination, unidirectional current-, and oscillation ripple-lamination, as well as dm-scale soft sediment deformation, maximum individual bed thickness 60 cm | VF – F | Upper shoreface to beach deposits with tidal influence | Curtis Fm. |
| H | Tangential cross-stratified gravelly sandstone | Matrix-supported conglomeratic dune, hm-scale lateral extent, sub-horizontal erosive base, rip-up mud clasts, extra-basinal sub- to rounded clasts, maximum clast Ø 2.5 cm, unidirectional-current trough cross-stratification, maximum individual dune thickness 2.50 m | M – Gr | High energy, asymmetric tidal flow pattern within a laterally restricted embayment | Curtis Fm. |

(Continues)

**TABLE 1** (Continued)

| Facies | Description | Structures | Grain size | Interpretation | Formation |
|---|---|---|---|---|---|
| I | Tidally-influenced cross-stratified conglomeratic sandstone | Matrix- to clast-supported lens-shaped intraformational conglomerate of restricted lateral extent, locally developed and amalgamated in tidal bundles, rip-up mud clasts, extra-basinal sub- to rounded clasts, maximum clast Ø 2.5 cm, bidirectional cross-stratification with superimposed current-ripples, maximum bed thickness 60 cm | F – Gr | High energy tidal channels-inlets | Curtis Fm. |
| J | Planar to sigmoidal cross-stratified sandy conglomerate | Clast- to matrix-supported conglomerate, hm-scale lateral extent, convex-down erosive base, flat top, extra-basinal sub- to rounded clasts, maximum clast Ø 2.5 cm, planar cross-stratification, maximum individual thickness 3.00 m | M – Gr | Point bar lateral accretion within a migrating tidal channel | Curtis Fm. |
| K | Plane parallel-laminated mud- to siltstone | Plane parallel-laminated mud- to siltstone, scattered bidirectional current ripple cross-stratifications grey to green, occasional desiccation cracks, sporadic bioturbations both parallel and normal to the bedding planes | Si – Cl | Gentle flow activity with tidally-related current reversals | Curtis Fm. |
| L | Heterolithic silt- and sandstone with lenticular bedding | Rippled vf-f grained sandstone, greyish lenses containing herringbone and current ripple cross-stratifications within a matrix of laminated grey to green mud- to siltstones, occasional desiccation cracks, sporadic bioturbations both parallel and normal to the bedding planes | Si – F | Current reversals in lower subtidal zone | Curtis Fm. |
| M | Heterolithic silt- and sandstone with wavy bedding | Ripple cross-stratified vf-f grained greyish sand layers, with bi-directional current indicators and interbedded with laminated grey to green siltstone, occasional desiccation cracks, sporadic bioturbations both parallel and normal to the bedding planes, varying amount of organic matter | Si – F | Current reversals in subtidal zone (shallower than Facies L) | Curtis Fm. Moab Mbr. |
| N | Heterolithic sandstone with flaser bedding | Ripple and herringbone cross-stratified vf-f grey to green to white sandstone, scattered mud lenses, as well as single and double mud drapes, varying amount of organic matter | VF – F | Upper sub- to lower intertidal sandflat | Curtis Fm. |
| O | Sandstone with climbing ripples | Climbing ripple cross-stratified vf-f grained sandstone, grey to green | VF – F | Tidal channel overbank spill on tidal flat, Upper sub- to lower intertidal sandflat | Curtis Fm. |
| P | Cross-stratified sandstone arranged in well-defined rhythmic tidal bundles | Vf-f(-m) grained grey to green to white sandstone, arranged in tidal bundles, with occasional anti-ripples documented from their toesets, varying amount of organic matter | VF – F (-M) | Tidal inlets, lower energy than Facies I | Curtis Fm. |

(Continues)

**TABLE 1** (Continued)

| Facies | Description | Structures | Grain size | Interpretation | Formation |
|---|---|---|---|---|---|
| Q | Structureless sandstone | Vf-f grained grey to green to white sandstone, massive, with potential scattered single and-or double mud drapes. Usually rounded and smoothly weathered | VF – F | The lack of structure might only be due to intensive surface weathering. Presence of mud drapes indicate sub- or intertidal environment | Curtis Fm. |
| R | Thoroughly bi-directional rippled cross-stratified sandstone | Thoroughly rippled silt- to vf-grained sandstone, dominated by herringbone cross-stratifications, potential climbing ripples | S – VF | Deep subtidal environment with near equal flood and ebb tidal current conditions. Note that the weathering can in some cases erase most of the sedimentary structures | Curtis Fm. Moab Mbr. |
| S | Plane parallel-stratified sandstone | Plane parallel-stratified vf-f-grained sandstone with scattered current ripple lamination, white, pink or green. Note that the weathering expression of this facies varies between the different units of the Curtis Fm. Potential mud cracks and soft sediment deformations | (S -) VF – F | Tidal sandflat, upper flow regime (to lower antidune-regime?). Documented mud cracks indicate short-lived subaerial exposure | Curtis Fm. Moab Mbr. |
| T | Condensed sandstone | Thin, yellow structureless sandstone, occasionally displaying low-amplitude undulations, exclusively observed capping the Moab Tongue Member of the Curtis Fm. Maximum bed thickness 10 cm | (VF-F -) F | Condensed horizon | Moab Mbr. |
| U | Rippled cross-stratified sandstone | Undulated to rippled cross-stratified vf-f-grained, grey to brown sandstone, with 3D current ripples, possible interference ripples, potential mud cracks and soft sediment deformations | VF – F | 3D migrating ripples under unidirectional current conditions | Entrada Ss Curtis Fm. Moab Mbr. Summerville Fm. |
| V | Plane parallel-laminated siltstone | Dark red soft slope forming siltstone, most probably plane parallel-laminated, scattered pale white bleached lenses and evaporites | Si | Supratidal plain | Summerville Fm. |
| W | Iron rich ripple- and parallel-laminated sandstone | Dark red to brown cemented vf-f-grained sandstone, gentle ripple cross-stratifications, potential desiccation cracks | VF – F | Fluvial overbank deposits | Summerville Fm. |
| X | Palaeosol | Dark purple mud or silt | M-S | Sub-aerially exposed surface with superficial soil development | Entrada Ss, Curtis Fm. Moab Mbr. Summerville Fm. |

**TABLE 2** Facies associations for the Entrada Sandstone, Curtis Formation, and Summerville Formation

| Facies association | Depositional environment | Facies included | Formation |
|---|---|---|---|
| FA 1a | Coastal wet aeolian dune system (Kocurek & Havholm, 1993; Mountney, 2012), with episodic (marine) partial flooding of interdunes deposits and superficial development of soil- and vegetated horizons | A, C, X | Entrada Sandstone Slick Rock Mbr. |
| FA 1b | Coastal wet aeolian interdune and lower coastal plain system (Kocurek & Havholm, 1993; Mountney, 2012), with episodic (marine) partial flooding of interdunes deposits and superficial development of soil- and vegetated horizons | B, C, D, X | Entrada Sandstone earthy facies |
| FA 2 | Beach deposits to upper shoreface deposits, with potential associated tidal channels cut-and-fill | C, G, S, U | Curtis Fm. |
| FA 3a | Subtidal heterolithic mud-, silt- vf-grained sandstone, generally upward coarsening from laminated mudstone to wavy beddied sandstone, scarsely bioturbated | H, I, J, K, L, M | Curtis Fm. |
| FA 3b | Subtidal heterolithic vf- to f-grained sandstone generally upward coarsening from wavy- to flaser bedded sandstone, scarsely bioturbated | H, I, M, N | Curtis Fm. |
| FA 4a | Sandy tidal flat with correlative major tidal channels, with potential subaerial exposures | S, U, X | Curtis Fm. |
| FA 4b | Tidal channel infills and splays, distal correlative of FA 4a in the northern areas | C, H, I, L, M, N, S, U | Curtis Fm. |
| FA 5 | High energy, sub- to intertidal sand -dominated environments, encompassing tidal flats, tidal channels, tidal dunes and tidal bars | C, G, (K, L, M,) N, O, P, Q, R, S(, X) | Curtis Fm. |
| FA 6 | Upper intertidal heterolithic channels and flats complex, upward finning, with intermittent prolonged subaerial exposures and rare bioturbation, indicator of a more stressed environment than FA 3 | K, L, M, N, Q, S, U, X | Curtis Fm. |
| FA 7 | Coastal dry aeolian dune field (Mountney, 2012), arranged in five sequences separated by supersurfaces, upon which transgressive water-carried sediments and/or palaeosol can be observed | A, N, Q, S, T, U, X | Curtis Fm. Moab Mbr. |
| FA 8 | Supratidal lower coastal plain, with episodic marine flooding | U, V, W, X | Summerville Fm. |

parallel-laminated to mottled siltstone and very fine-grained sandstone, with interdigitating trough cross-stratified sandstone, rippled cross-stratified sandstone, evaporitic beds and isolated dunes (Figures 3a, b and 4, Table 2). FA 1b thickens north-westwards, and pinches out southwards around Notom Ranch (35), and eastwards in the vicinity of Moab (Figure 2). Processed gamma-ray data from Duma Point (19) (Figure 5) provide thorium/uranium ratios of approximately 5.

FA 1 is capped by the polygenetic, heterochronous, and diachronous (Zuchuat et al., in press) J-3 Unconformity of Pipiringos and O'Sullivan (1978). Locally, erosive scours at the top of the FA 1b are infilled with matrix-supported, chaotically arranged conglomerates, comprising rounded to well-rounded extra-basinal pebbles and cobbles (Figure 6a–c).

## 4.1.2 | Interpretation

FA 1a corresponds to a coastal wet aeolian dune system (after Mountney, 2012), whereas the contemporaneous FA 1b strata were deposited within a marginal-marine, sabkha-like environment at the fringe of the Slick Rock Member palaeo-erg, where isolated coastal aeolian dunes migrated and loess were intermittently deposited. The erosive scours at the top of the unit are interpreted as the product of flash floods predating the transgression of the Curtis Sea, and the accompanied deposits settled as the flows decelerated. Except for these flash flood deposits and some episodic fluvial terminal splays (Valenza, 2016), evidence for major fluvial development is lacking within the Entrada Sandstone. The thorium/uranium ratios of 5 suggest a more prominent marine origin for these sediments, rather than a fully continental provenance (Fertl et al., 1982).

## 4.2 | FA 2 – Beach to upper shoreface deposits

### 4.2.1 | Description

In the northern and western parts of the study area, notably at Sven's Gulch (9), Interstate 70 (12) and Shadscale Mesa (13), the surface of the J-3 Unconformity was locally modified as an approximately 2 m thick, laterally restricted (200–500 m) fine-grained sandstone (FA 2; Figures 3c and 4, Table 2), locally deforming its substratum by loading. The lowermost sandstones are plane parallel-stratified and planar to low-angle cross-stratified, which are overlain by trough cross-stratified sandstone and/or ripple-laminated sandstone. Mud drapes and rip-up clasts are documented at Interstate 70 (12) and Uneva Mine Canyon (14). FA 2 overlies FA 1, from which it is separated by the J-3 unconformity, which can locally display loading structures (Figure 3c).

### 4.2.2 | Interpretation

FA 2 represents tidally-influenced upper shoreface deposits. These upper shoreface deposits represent the oldest deposits of the Curtis Formation (Zuchuat et al., 2018).

## 4.3 | FA 3 – Subtidal heterolithic flat

### 4.3.1 | Description

Sediments of FA 3 overlay FA 2 (or the J-3 unconformity where FA 2 is not present) and are dominated by thinly bedded and laterally extensive, heterolithic subtidal deposits, with a varying sand-to-mud ratio, ranging from mud-dominated (FA 3a), commonly observed in the northern, more distal part of the system, to sand-dominated (FA 3b), prevailing in the more proximal and southern part of the shallow-marine basin (Figures 3d and 4; Table 2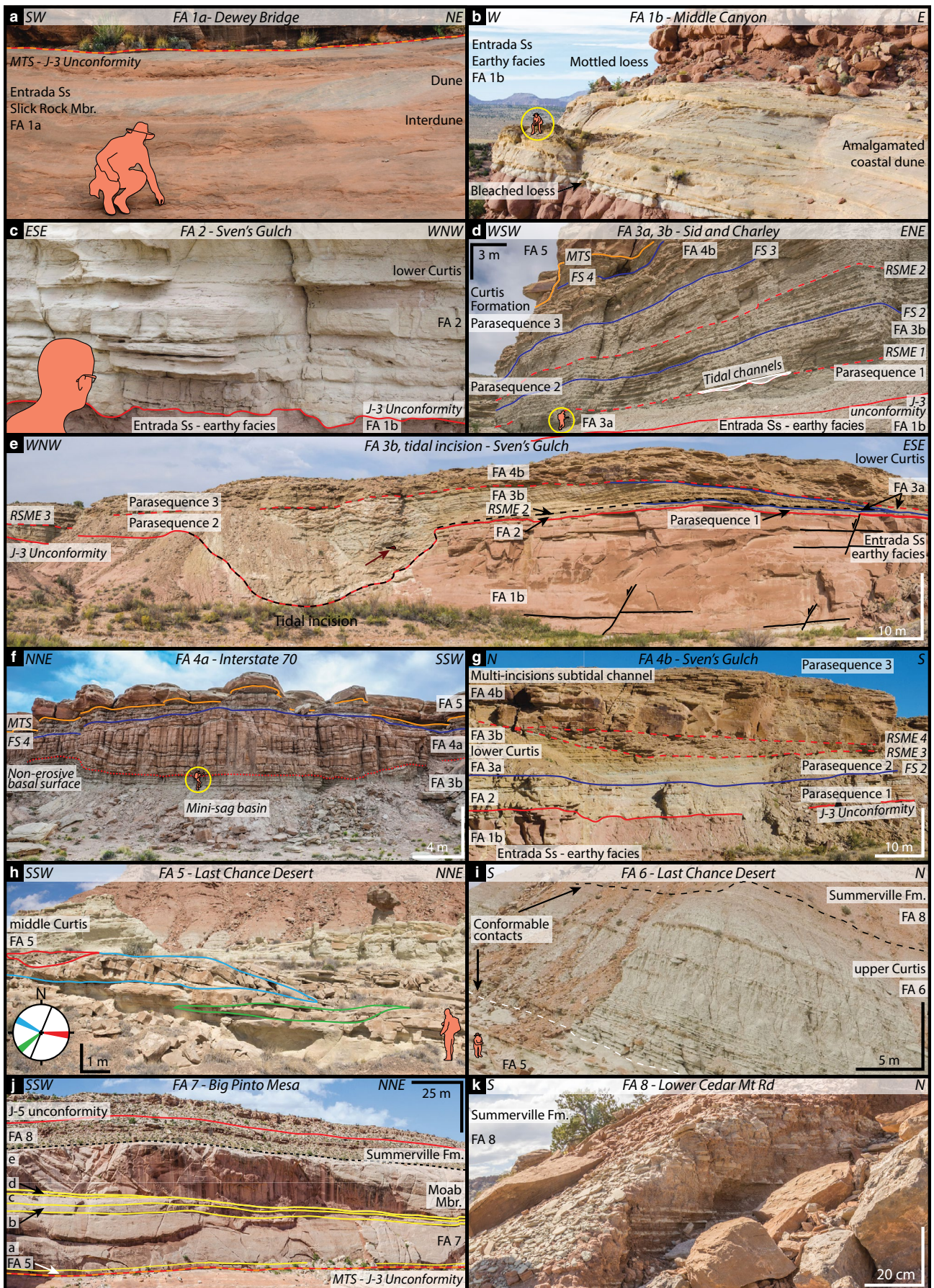). FA 3 is characterized by abundant, bi-directional ripple cross-laminated, cross-stratified, lenticular to flaser-bedded siltstone and sandstone strata (Figure 7a–c). A bed typically reaches thicknesses of 3–10 cm. The base of FA 3a can be gradational, or it corresponds to a sharp and sometimes erosive surface. The base of FA 3b is either conformable, as visible in the more distal and deeper part of the system in the north (Figure 4) where up to three stacked successions gradually transition and coarsen upward from FA 3a to FA3b. It can also correspond to a regressive surface of marine erosion in the proximal part of the study area, capable of cutting 45 m wide and 10 m deep incisions into its substrata (Figure 3e). Despite their intraformational erosive character, deposits of FA 3a and FA 3b are often preserved passively onlapping the J-3 Unconformity, as they don't erode into the underlying strata of the Entrada Sandstone (Zuchuat et al., in press).

In the north of the study area, cross-stratified, heterolithic, bedforms, with concave up, erosive bases and flat upper surfaces (Figure 6a, d) form part of FA3. The infills comprise rounded to well-rounded, gravel-size, extra-basinal clasts within a matrix of fine to very coarse-grained sand, with green mud drapes locally observed between the gravelly foresets (Figure 7d). Heterolithic gravelly dunes arranged in thin-thick-thin cyclical bundles, with centimetre-thick mud drapes between foresets (Figure 6a,e) are also present. These deposits are characterized by a sharp but non-erosive flat base, and concave down top surface, migrating on FA 3 substrata.

### 4.3.2 | Interpretation

FA 3 heterolithic deposits testify of oscillating energy within the system (Kvale, 2012). The three upward-coarsening trends observed notably in the northern part of the study area (Figure 4) indicate an increasing energy level within a gradually shallowing subtidal flat environment. Each of the three upward shallowing packages are bounded by flooding surfaces, and are interpreted as parasequences, sensu Catuneanu et al. (2009). In the more

---

**FIGURE 3** Summary panel of the Facies Associations (FA) cropping out within the study area. (a) Example of wet coastal aeolian dunes of FA 1a (Entrada Sandstone, Slick Rock Member). (b) Amalgamated aeolian coastal dunes within the fine-grained, marginal marine earthy facies of FA1b (Entrada Sandstone). Note the bleached horizon directly below the dunes. Geologist for scale. (c) High-energy upper shoreface to beach deposits, with rip-up clasts and occasional mud drapes. Note the loaded and eroded irregular geometry of the J-3 Unconformity. (d) Typical stacking architecture of subtidal mud- (FA 3a) and sand-dominated heterolithic flat deposits (FA 3b). (e) Major tidal incision observed at Sven's Gulch, carved during a short-lived regressive phase within Parasequence 2. The dark red arrow points at a boulder of Entrada Sandstone within a matrix of FA 3b sand-dominated deposits. Note also the ravinement of Parasequence 2 deposits during the transgressive phase of Parasequence 3, followed by the by the development of a regressive and erosive, subtidal channel complex (FA 4b). (f) Mini sag basin generated by the collapse of FA 3b deposits, as FA 4a sand-rich subtidal to supratidal sandflat was being deposited. (g) Two incision phases of FA 4b subtidal channel. (h) Bidirectional tidal inlets (red and blue contours), and a third south-westward laterally accreting tidal channel (green contour) within a subtidal to intertidal flat surrounding environment (FA 5). The respective migration direction of these three bedforms is colour-coded on the rose-diagram, whereas the black line on the diagram illustrates the outcrop orientation. (i) Conformable contact between the underlying FA 5 subtidal to intertidal channel-dune-flat complex, grading into the thinner and finer-grained FA 6 upper subtidal to intertidal deposits, which are conformably overlain by FA 8 supratidal deposits of the Summerville Formation. (j) Five aeolian sequences recorded in the Moab Member of the Curtis Formation. (k) Close-up images of FA 8 supratidal deposits displaying regular episodes of marine flooding (white sandstone beds)
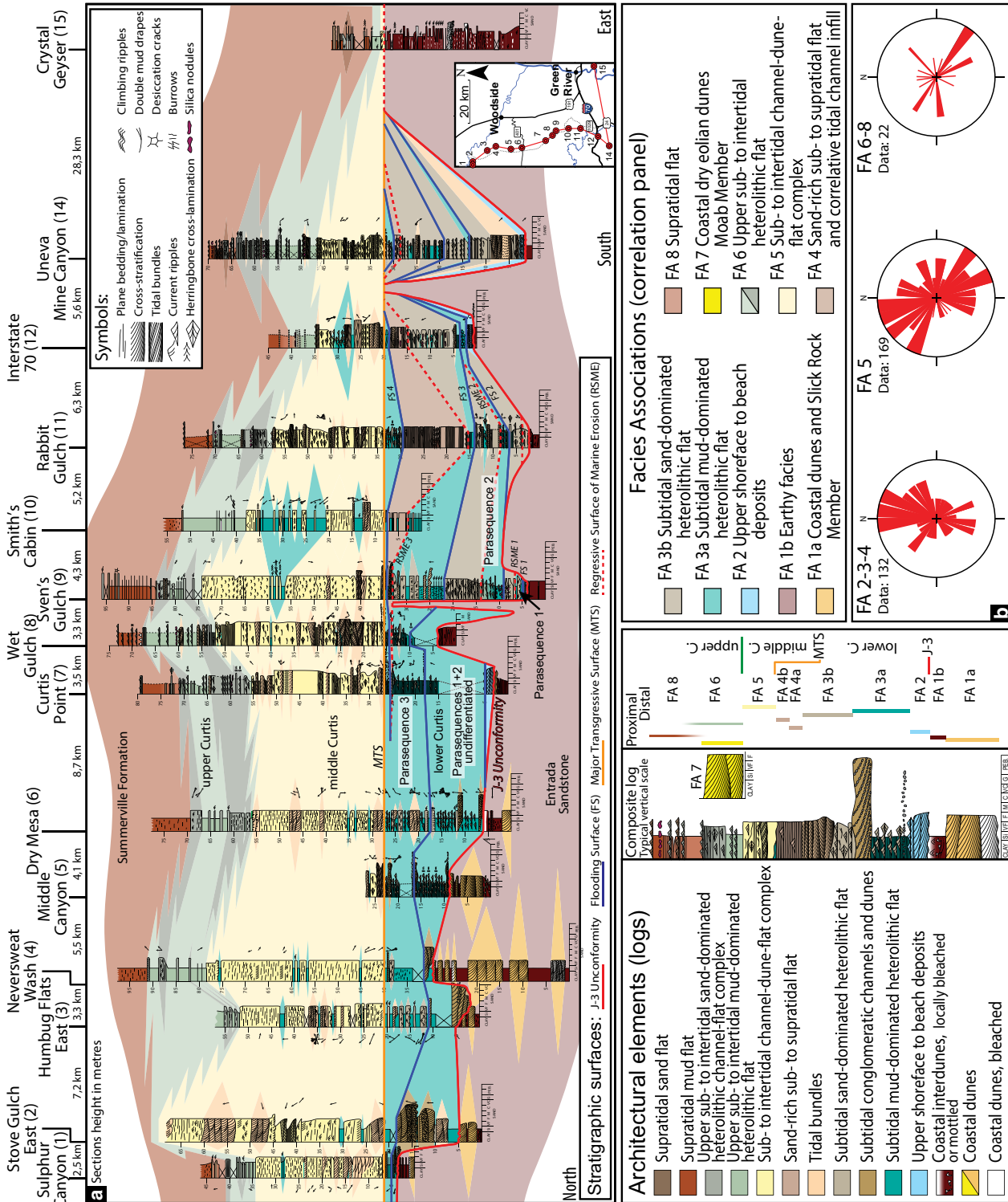
**a** SW — FA 1a - Dewey Bridge — NE
MTS - J-3 Unconformity
Entrada Ss
Slick Rock Mbr.
FA 1a
Dune
Interdune

**b** W — FA 1b - Middle Canyon — E
Entrada Ss
Earthy facies
FA 1b
Mottled loess
Amalgamated coastal dune
Bleached loess

**c** ESE — FA 2 - Sven's Gulch — WNW
lower Curtis
FA 2
J-3 Unconformity
Entrada Ss - earthy facies
FA 1b

**d** WSW — FA 3a, 3b - Sid and Charley — ENE
3 m
FA 5
MTS
FS 4
Curtis Formation
Parasequence 3
FA 4b
FS 3
RSME 2
FS 2
FA 3b
RSME 1
Parasequence 2
Parasequence 1
Tidal channels
J-3 unconformity
FA 3a
Entrada Ss - earthy facies
FA 1b

**e** WNW — FA 3b, tidal incision - Sven's Gulch — ESE
lower Curtis
FA 3a
RSME 3
Parasequence 3
Parasequence 2
FA 4b
FA 3b
RSME 2
FA 2
Parasequence 1
Entrada Ss earthy facies
J-3 Unconformity
FA 1b
Tidal incision
10 m

**f** NNE — FA 4a - Interstate 70 — SSW
FA 5
MTS
FS 4
FA 4a
Non-erosive basal surface
Mini-sag basin
FA 3b
4 m

**g** N — FA 4b - Sven's Gulch — S
Parasequence 3
Multi-incisions subtidal channel
FA 4b
FA 3b
lower Curtis
FA 3a
FA 2
FA 1b
RSME 4
RSME 3
Parasequence 2
FS 2
Parasequence 1
J-3 Unconformity
Entrada Ss - earthy facies
10 m

**h** SSW — FA 5 - Last Chance Desert — NNE
middle Curtis
FA 5
N
1 m

**i** S — FA 6 - Last Chance Desert — N
Summerville Fm.
FA 8
Conformable contacts
upper Curtis
FA 6
FA 5
5 m

**j** SSW — FA 7 - Big Pinto Mesa — NNE
25 m
J-5 unconformity
FA 8
e
d
c
b
a
FA 5
Summerville Fm.
Moab Mbr.
FA 7
MTS - J-3 Unconformity

**k** S — FA 8 - Lower Cedar Mt Rd — N
Summerville Fm.
FA 8
20 cm

**FIGURE 4** (a) N–S–W oriented correlation panel along the NW margin of the San Rafael Swell, and the correlative spatial distribution of facies associations across the Curtis Basin. The datum corresponds to the Major Transgressive Surface (MTS). (b) Rose diagrams displaying the palaeocurrent measurements for the lower Curtis (FA 2, FA 3, and FA 4), the middle Curtis (FA 5), and the upper Curtis–Summerville Formation intervals (FA 6 and FA 8)

proximal part of the shallow-marine system, the erosive surfaces, sometimes observed at the base of the FA 3b, correspond to regressive surfaces of marine erosion (RSME; Figure 4). These RSMEs result from the basinward migration of subtidal environments characterized by higher energy conditions accompanying the development of the above mentioned parasequences. The occurrence of RSME's in the more proximal part of the system, contrasting with their notable absence in the deeper and more distal part of the basin, denotes a basinward-increasing slope gradient. The bedforms, with concave up, erosive bases and flat upper surfaces (Figure 6a,d) are interpreted as subtidal channels. Their restricted occurrence in the more distal and basinward part of the system, interbedded between mud-dominated heterolithic deposits of FA 3a (Figure 4), highlights the separation of the flow in the system. This is in contrast to the unseparated and relatively higher energy conditions observed in the more proximal parts of the basin to the south, which otherwise lead to the deposition of better sorted sediments (FA 3b).

## 4.4 | FA 4 – Sand-rich subtidal to supratidal flat and correlative tidal channel infill

### 4.4.1 | Description

FA 4 is subdivided into FA 4a and FA 4b. FA 4a comprises light-pink, very fine to fine-grained sandstones that extend over tens of kilometres on the eastern margin of the San Rafael Swell, in the southern and more proximal part of the study area (Figures 2 and 3f). FA 4a is characterized by a southward thickening (from 4 to 15 m thick) of plane parallel-bedded to plane parallel-laminated strata, with single and double mud drapes, along with rare, unidirectional current ripples and herringbone cross-stratification.

Fa 4b is restricted to the north-eastern margin of the San Rafael Swell, where it consists of a 1–10 m thick, multi-storey, coarse-grained, cross-stratified sandstone with rounded to well rounded, gravel size extra-basinal clasts (Figure 3g). It displays common mud drapes along foresets, reactivation surfaces, as well as bidirectional current indicators, such as subordinate-flow ripples climbing on the reactivation surfaces, and herringbone cross-stratification.

### 4.4.2 | Interpretation

FA 4a and FA 4b represent a proximal subtidal to supratidal sandflat, and the correlative, more distal, gravel-rich, subtidal channels, respectively (Table 2). FA 4 occurs only within the uppermost parasequence of the lower Curtis (Parasequence 3). The grainsize and the colour of FA 4a are potentially related to the reworking of fringing deposits of the contemporaneous and neighbouring aeolian dune fields of the Slick Rock

Member. FA 4 is interpreted to reflect the most prominent basinward shoreline progradation recorded by the lower Curtis, constituted by FA 2, FA 3, and FA 4. The lowermost parasequence, occurs only at Sven's Gulch (9), Cedar Mountain (43), and Sid and Charley (41) (Figure 3d). It is characterized by steep tidal incisions (Figure 3e). Despite evidence of current reversals within the sediments (Figure 7a,c), the lower Curtis is dominated by a basinward (northward) current direction (Figure 4b).
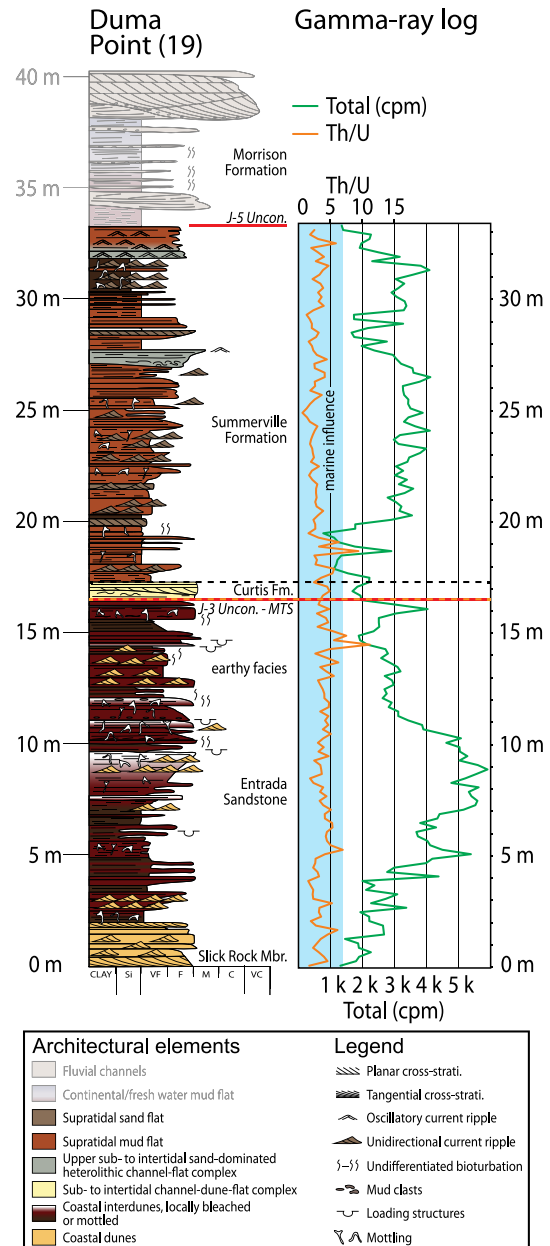


**FIGURE 5** Duma Point sedimentary section and associated cyclical gamma-ray log. The thorium/uranium (Th/U) values generally fall below 7 at approximately 5, which suggest a more prominent marine origin for these sediments, rather than a fully continental provenance (Fertl et al., 1982). The Morrison Formation is shaded as it is not of interest for this study. See Figure 2 for section location. Contains BGS Data © UKRI 2019.

**FIGURE 6**  (a) Three different conglomeratic deposits observable within the lower Curtis unit. Note the waxing-waning bundle arrangement of the upper gravelly channel and the absence of similar structure in the gravelly dunes. (b, c) Close-up of the basal flash flood pebbly conglomerate, overlain by a gravelly dune. (d) Lateral migration of a sinuous subtidal, gravelly channel. Note its concave up, erosive base and flat upper surface (see Figure 10 for detail architectural arrangement of that subtidal channel). (e) Gravelly dune, arranged in waxing-waning bundles, migrating over subtidal, mud-dominated heterolithic flat deposits (FA 3a)

## 4.5 | FA 5 – Subtidal to intertidal channel-dune-flat complex description

### 4.5.1 | Description

The lower Curtis is overlain disconformably by FA 5 (Figures 3h and 4a, Table 2) which represents the informal middle Curtis unit (Zuchuat et al., 2018). Its base is sharp, and it can be erosive. It can be traced throughout the study area, all the way to Ghost Ranch, northern New Mexico, where it marks the base of the Todilto Member of the Wanakah Formation (Figure 2; Zuchuat et al., 2018, in press). The thickness of FA 5 varies from more than 45 m in the northern part of the study area, to approximately 1 m, as it thins south and eastwards. These sediments comprise light green to white, very fine to fine-grained well-sorted sandstone (Figure 7e–i). Grain size fines slightly south and eastwards, where FA 5 is dominated by very fine to fine-grained sandstone. FA 5 features lenticular to wavy to flaser-bedded sandstones, with occasional laminated mudstones. It also comprises climbing ripples, and intervals dominated by bidirectional herringbone cross-stratification. Interference ripples occur sporadically within the succession, arranged in a near orthogonal pattern. 3D cross-stratified packages are observed within FA 5, with frequent reactivation surfaces and counter-ripples. The cross-stratified and wavy to flaser-bedded sandstone strata are locally arranged in centimetre to metre-scale tidal bundles with varying amounts of organic/argillaceous matter, often deposited as single or double mud drapes. FA 5 also comprises plane parallel-stratified, and low-angle cross-stratified intervals. These facies laterally interdigitate with one another over distances of 5–40 m. Individual bedforms in FA 5 reach a maximum height of 2–3 m, and the average bedform size is one to two orders of magnitude higher than in the underlying lower Curtis deposits. Bedform thickness decreases up-section, as well as south and eastwards, as FA 5 thins in these directions. Palaeocurrent measurements indicate a strong bi-modal distribution of current motion at the time of deposition, oriented NW-SE (Figure 4b).

### 4.5.2 | Interpretation

FA 5 corresponds to the informal middle Curtis unit (Zuchuat et al., 2018). Its basal surface corresponds to the MTS, which is a composite transgressive-ravinement surface. FA 5 is interpreted as an intricate amalgamation of subtidal to intertidal channels and associated tangential to sigmoidal cross-stratified sandstones arranged in tidal bundles. This indicates strong cyclical tidal influence on the system with a dominant bidirectional current component. Subtidal channels eroded into sandflats and subaqueous 3D dunes within a subtidal to intertidal system. FA 5 reflects an overall higher energy level, evidenced by coarser-grained and better-sorted sediments than compared with the underlying lower Curtis strata. The amalgamated bedforms and bedform sets inhibits the recognition of any traceable stratigraphic surfaces, such as flooding surfaces or regressive surfaces of marine erosion, accentuating the contrast with the underlying lower Curtis shallow-marine system.

## 4.6 | FA 6 – Upper heterolithic subtidal to intertidal flat

### 4.6.1 | Description

The middle Curtis FA 5 deposits are conformably overlain by FA 6, which consists of green, siltstone to fine-grained, laterally extensive, isopachous sandstone beds, distinguished by plane parallel stratification, unidirectional current ripple and herringbone cross-stratification. Individual bed set thicknesses range from 3 to 40 cm, and beds become thinner up-section (Figure 3i, Table 2). FA 6 crops out in the northern, central, and southern parts of the study area (Figures 4 and 8; Zuchuat et al., 2018). Unlike the underlying sediments of FA5, FA 6 thins northwards, from a maximum thickness of approximately 28 m near Hanksville (34) to a minimum of 5 m at Sulphur Canyon (1) (Figure 4).

### 4.6.2 | Interpretation

FA 6 constitutes the informal upper Curtis, conformably overlying the middle Curtis (Zuchuat et al., 2018). It was deposited within subtidal to intertidal flat environments (Figure 3i, Table 2), reflecting a lower energy environment with respect to those of the underlying FA 5.

## 4.7 | FA 7 – Coastal dry eolian dune field

### 4.7.1 | Description

Towards the eastern part of the study area, FA 6 is replaced by FA 7, (Figures 3j and 8, Table 2). FA 7 reaches a maximum
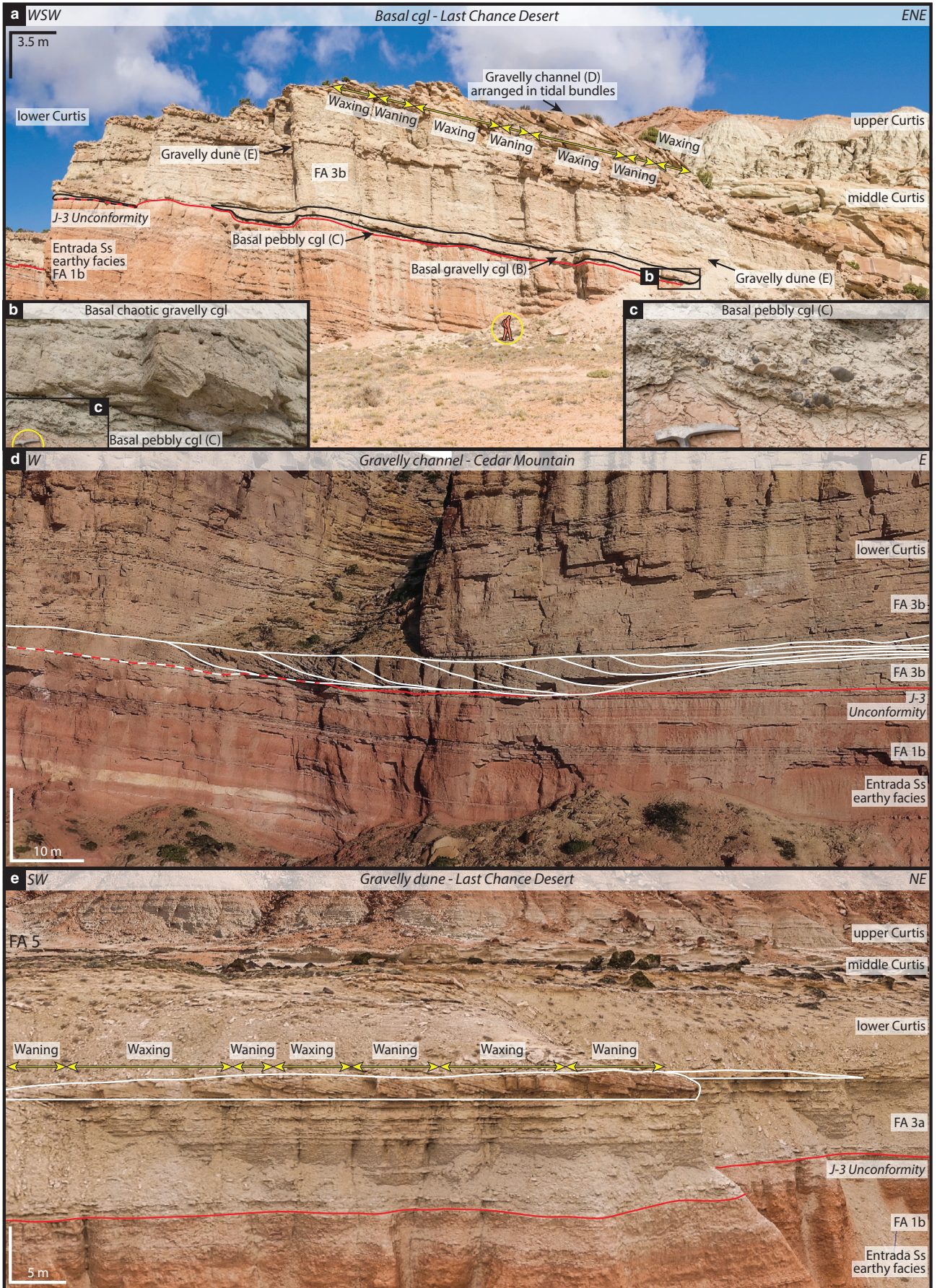
**a** WSW — Basal cgl - Last Chance Desert — ENE

3.5 m

lower Curtis
upper Curtis
Gravelly channel (D) arranged in tidal bundles
Waxing Waning Waxing Waning Waxing Waning Waxing Waning Waxing
Gravelly dune (E)
middle Curtis
FA 3b
J-3 Unconformity
Entrada Ss earthy facies FA 1b
Basal pebbly cgl (C)
Basal gravelly cgl (B)
**b**
Gravelly dune (E)

**b** Basal chaotic gravelly cgl
**c**
Basal pebbly cgl (C)

**c** Basal pebbly cgl (C)

**d** W — Gravelly channel - Cedar Mountain — E

lower Curtis
FA 3b
FA 3b
J-3 Unconformity
FA 1b
Entrada Ss earthy facies
10 m

**e** SW — Gravelly dune - Last Chance Desert — NE

FA 5
upper Curtis
middle Curtis
lower Curtis
Waning Waxing Waning Waxing Waning Waxing Waning
FA 3a
J-3 Unconformity
FA 1b
Entrada Ss earthy facies
5 m

**FIGURE 7** Common tide-dominated and tidally-modulated bedforms present in the Curtis Formation. See Facies Table 1 for codes. (a) Bi-directional rippled cross-stratified sandstone (Facies R). (b) Heterolithic siltstone and sandstone with lenticular (LB) and wavy bedding (WB) (Facies L, M). (c) Bi-directional rippled cross-stratified sandstone with episodic climbing ripples (Facies R). (d) Tangential cross-stratified gravelly sandstone (Facies H), thought to result from tidally-reworked flash flood deposits, migrating over a sole of mud- to sand-dominated heterolithic deposits (FA 3). (e) Heterolithic siltstone and sandstone with wavy and flaser bedding (FB) (Facies M, N), arranged in rhythmic tidal bundle. (f) Tangential cross-stratified sandstone (Facies C), with rippled reactivation surfaces, mud drapes and rip-up mud clasts. (g) Cross-stratified sandstone arranged in well-defined rhythmic tidal bundles (Facies P). (h) Heterolithic sandstone with flaser bedding (Facies N), arranged in rhythmic tidal bundle. (i) Organic-rich (OM) toesets of a cross-stratified sandstone arranged in well-defined rhythmic tidal bundles (TB) (Facies P)

thickness of approximately 50 m close to the Utah–Colorado border, and pinches out between Duma Point (19) and Horse Flies Gulch (20). It is characterized, at its base, by very fine to fine-grained, structureless to ripple to trough cross-stratified sandstones, interbedded with green silty sandstones, commonly displaying soft sediment deformation structures. FA 7 is composed of five packages of fine-grained, cross-stratified dunes, reaching an individual maximum thickness of approximately 15–20 m at Lost Spring Canyon (28) on the eastern border of Arches National Park. Each package is capped by a traceable erosive surface, under which abundant rhizoliths can be observed (Zuchuat et al., 2018). These erosive surfaces can be overlain by very fine to fine-grained, ripple or herringbone cross-stratified sandstones with single and double mud drapes, and arranged in flaser-bedded packages. Undulating millimetre to centimetre-scale, structureless sandstone strata also occur on top of these erosive surfaces. The uppermost package is also overlain by a thin sandstone crust that is typically structureless.

### 4.7.2 | Interpretation

FA 7 consists of aeolian dunes corresponding to Doelling's (2001) Moab Member of the Curtis Formation (Figures 3j and 8, Table 2). The traceable erosive truncations are supersurfaces (sensu Kocurek, 1988), implying that the Moab Member consists of five stacked aeolian sequences. Towards Duma Point (19), subtidal to intertidal deposits are commonly found overlying these supersurfaces, whereas supratidal deposits become more frequent towards the eastern and more continental part of the study area, linked with the development of local sand stromatolite structures similar to those described by Getty and Hagadorn (2009). These supratidal deposits are often associated with sparsely vegetated palaeosol horizons, as testified by the development of rhizoliths in the underlying strata.

### 4.8 | FA 8 – Supratidal flat

### 4.8.1 | Description

FA 8 consists of rusty red to dark brown, evaporite-rich mudstones and siltstone deposits that sharply overly the aeolian dunes of FA 7. The contact between FA 8 and the underlying

strata of FA 6 subtidal to supratidal sediments is gradational (Figure 3i,k, Table 2). FA 8 also contains centimetre to decimetre-thick, light grey, ripple cross-stratified sandstone beds. The thickness and the frequency of these deposits diminish up-section. Similarly to FA 1b, the thorium/uranium ratios processed from the gamma-ray data collected at Duma Point (19) fall at approximately 5. Only three minor channels were observed within FA 8, reaching 30–50 m in width, and 0.5–1 m in depth.
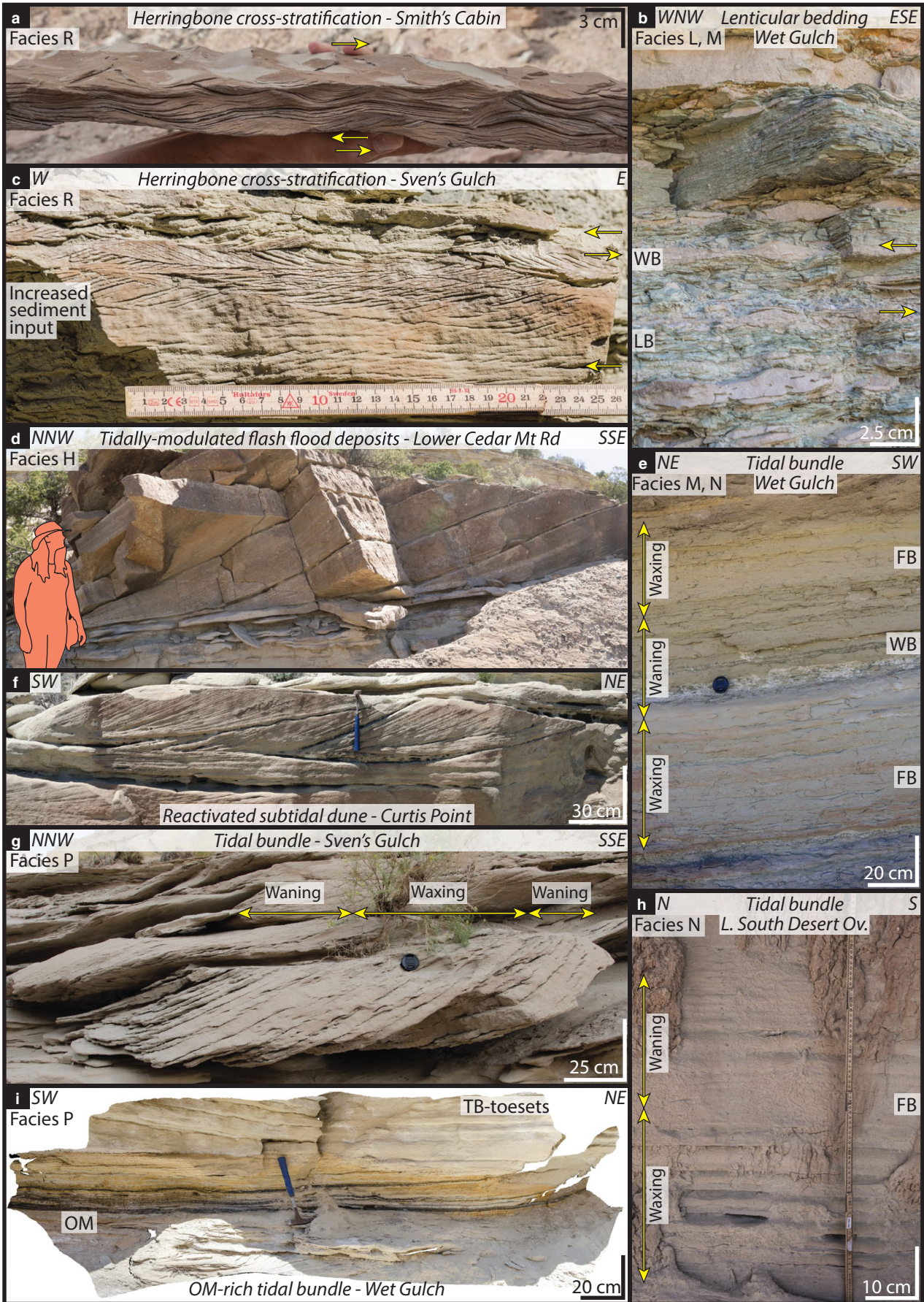
### 4.8.2 | Interpretation

FA 8 belongs to the Summerville Formation, and mainly consists of fine-grained supratidal, paralic to sabkha-like sediments that overly the shallow-marine deposits of the Curtis Formation. These were likely deposited as the Curtis Sea regressed. The occurrence of light grey, marine-influenced strata testifies to the frequent and recurrent marine incursions that punctuated overall regression. The marine influence of FA 8 is supported by thorium/uranium values of approximately 5, similar to values observed in FA 1b. The fluvially starved aspect of the studied basin is further emphasized by the scarcity and the limited size of the fluvial channels observed in outcrop within this paralic system, contemporaneous to the neighbouring shallow-marine domain.

### 4.9 | Unconformity

### 4.9.1 | Description

The J-3 Unconformity, which separates the Entrada Sandstone from the Curtis Formation is characterized by eight different types of relief related to (a) erosive or (b) deformation-related processes. The different types of relief are classified as (a) angular unconformity, (b) paraconformity, (c) steep incisions, (d) undulating relief, (e) irregular relief, including fault-plane and erosion-related relief irregularities, (f) circular collapsed structures, (g) sedimentary loading, and (h) hydroplastic sagging (Zuchuat et al., in press). The relief ranges from a centimetre-scale, to a maximum amplitude of 23 m, whereas its wavelength can reach 200 m (Zuchuat et al., in press). To the east of the study area, the J-3 Unconformity merges with the MTS at the base of the middle Curtis.

**a** Facies R — *Herringbone cross-stratification - Smith's Cabin* — 3 cm

**b** WNW — *Lenticular bedding* ESE — Facies L, M — *Wet Gulch* — WB, LB — 2.5 cm

**c** W — *Herringbone cross-stratification - Sven's Gulch* — E — Facies R — Increased sediment input — WB — LB

**d** NNW — *Tidally-modulated flash flood deposits - Lower Cedar Mt Rd* — SSE — Facies H

**e** NE — *Tidal bundle* — SW — Facies M, N — *Wet Gulch* — Waxing, Waning, Waxing — FB, WB, FB — 20 cm

**f** SW — NE — *Reactivated subtidal dune - Curtis Point* — 30 cm

**g** NNW — *Tidal bundle - Sven's Gulch* — SSE — Facies P — Waning, Waxing, Waning — 25 cm

**h** N — *Tidal bundle* — S — Facies N — *L. South Desert Ov.* — Waning, Waxing — FB — 10 cm

**i** SW — NE — Facies P — TB-toesets — OM — *OM-rich tidal bundle - Wet Gulch* — 20 cm

### 4.9.2 | Interpretation

The J-3 Unconformity composite surface is the product of a series of erosive processes, which includes aeolian deflation, superficial incision linked to flash floods, tidal ravinement during transgressive phases, and funnelling of the tidal forces as the shoreline regressed. It is important to notice that these different processes did not only impact the system in a 3D space, but they varied with time, both in terms of intensity and location. Furthermore, each individual process and individual type of relief are non-unique, as a specific relief geometry can be produced by different processes, and one single process can generate different geometries (Burgess & Prince, 2015; Zuchuat et al., in press). Therefore, the composite and highly polychronous nature of such a surface implies that it cannot be regarded as a genuine time barrier, and thus, as an unconformity sensu stricto.

## 5 | DEPOSITIONAL MODEL

Several authors have presented the Curtis and Summerville formations as an overall TR cycle (Caputo & Pryor, 1991; Peterson, 1994; Wilcox & Currie, 2008). This study supports their interpretation as a general conclusion, but the spatially and stratigraphically diverse body of data assembled here suggests that the detailed stratigraphic history of the interval is more intricate than that previously proposed (Figure 9). Importantly, in low-gradient systems like the Curtis basin the interpretation of stratigraphic detail is strongly influenced by the effects of relatively minor changes in sea level upon the position of the shoreline and, by consequence, the facies distribution (Midtkandal & Nystuen, 2009).

### 5.1 | Pre-Curtis Sea transgression

The J-3 Unconformity is intrinsically polygenetic, heterochronous, and diachronous by nature (Zuchuat et al., 2018, in press), comparable to the compound surface discussed by Ahokas, Nystuen, and Martinius (2014), as the deposition of the Entrada Sandstone, the Curtis, and Summerville formations, and the accompanying relative sea-level variations, all influenced the genesis of this bounding surface. Consequently, the J-3 Unconformity is not the product of a forced regression, as suggested by Mitchum, Vail, and Thompson's (1977) definition of unconformities, but was primarily developed as the Curtis Sea started to transgress from the north.

An interpretation of a composite, polygenetic, heterochronous, and diachronous J-3 Unconformity is further supported by preliminary gamma ray data obtained from the earthy facies of the Entrada Sandstone at Duma Point (19) (Figures 5 and 8). As thorium/uranium ratios of <7 can be used to indicate marine influences within sedimentary rocks

(Fertl et al., 1982), recorded values in this study of approximately 5 indicate marine influences over these paralic strata. $U_{excess}$ calculations clearly identify cyclical marine flooding (Figure 5) in the earthy facies of the Entrada Sandstone, but also in the supratidal deposits of the Summerville deposits. These lines of evidence together support an interpretation of the earthy facies as partly influenced by marine flooding as the early Curtis sea migrated southwards and into a coastal aeolian system in the south and eastern part of the study area (Figure 9a,b). This was accompanied by the development of the J-3 Unconformity as a ravinement surface (Zuchuat et al., in press), rather than an unconformity sensu stricto.

### 5.2 | Early Curtis Sea transgression

The oldest sediments of the Curtis Formation developed during the earliest flooding of the earthy facies, and correspond to FA 2 shoreface deposits. As these sedimentary bodies are constrained to certain localities (Curtis Point (7), Sven's Gulch (9), and Uneva Mine Canyon (14)), it can be regarded as evidence for pre-existing relief on the J-3 Unconformity, as palaeo-highs within the Entrada Sandstone acted as interfluves that remained unflooded until the subsequent transgression (Figure 9b). The exact nature of these palaeo-highs remains equivocal. Nevertheless, as FA 2 typically overlies deposits of the earthy facies (FA 1b), a purely sedimentary explanation for the existence of palaeo-topography seems unlikely. They could, however, be linked to pre-transgression, sub-regional folding and tilting episodes (Zuchuat et al., in press), which generated low amplitude and long wavelength relief.

The transgression continued, and reached areas around Hanksville, which represents the most proximal domain of the study area (Figures 2 and 9c). As transgression progressed, the energy of the system diminished and the subtidal heterolithic successions of FA 3 were deposited. The eastern part of the study area remained unaffected by the marine flooding. Sub-regional uplift episodes, coupled with the erosive nature of the MTS that accompanied deposition of the middle Curtis (Zuchuat et al., 2018, in press), mean that the western extent of the transgression remains unconstrained.

FA 3a mud-dominated deposits, which are more common in the northern parts of the study area, represent a tidally influenced distal domain of the Curtis Sea, whereas the coarser grained, sand-dominated FA 3b strata are concentrated towards the more proximal domain of tidal influence in the south (Figure 4; Zuchuat et al., 2018). The proximal sediments (FA3b) are characterized by better-sorted and coarser grained deposits compared to the distal setting (FA 3a). However, occasional localities within the more distal domain of the Curtis, such as Cedar Mountain (43), sometimes can display a succession dominated by FA 3b. Textural trends such as these, which show an increase in the degree of sorting
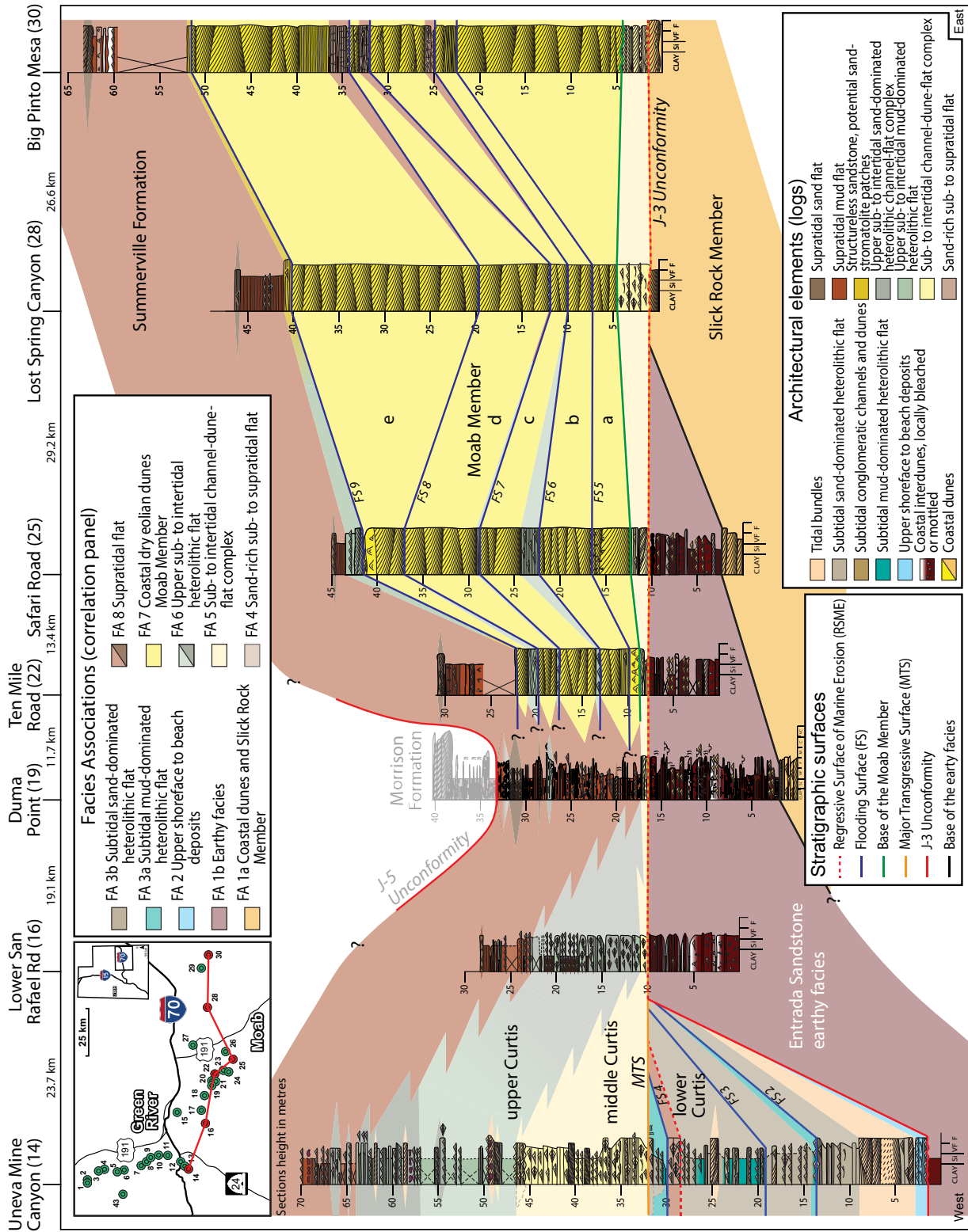
**FIGURE 8** E–W oriented correlation panel across the marine part and the aeolian Moab Member of the Curtis Formation. The datum corresponds to the Major Transgressive Surface (MTS). Note that the five, cyclical aeolian sequences identified in the Moab Member of the Curtis Formation suggest that the contemporaneous Summerville Formation could have undergone, and most probably underwent, similar cycles as it was being deposited
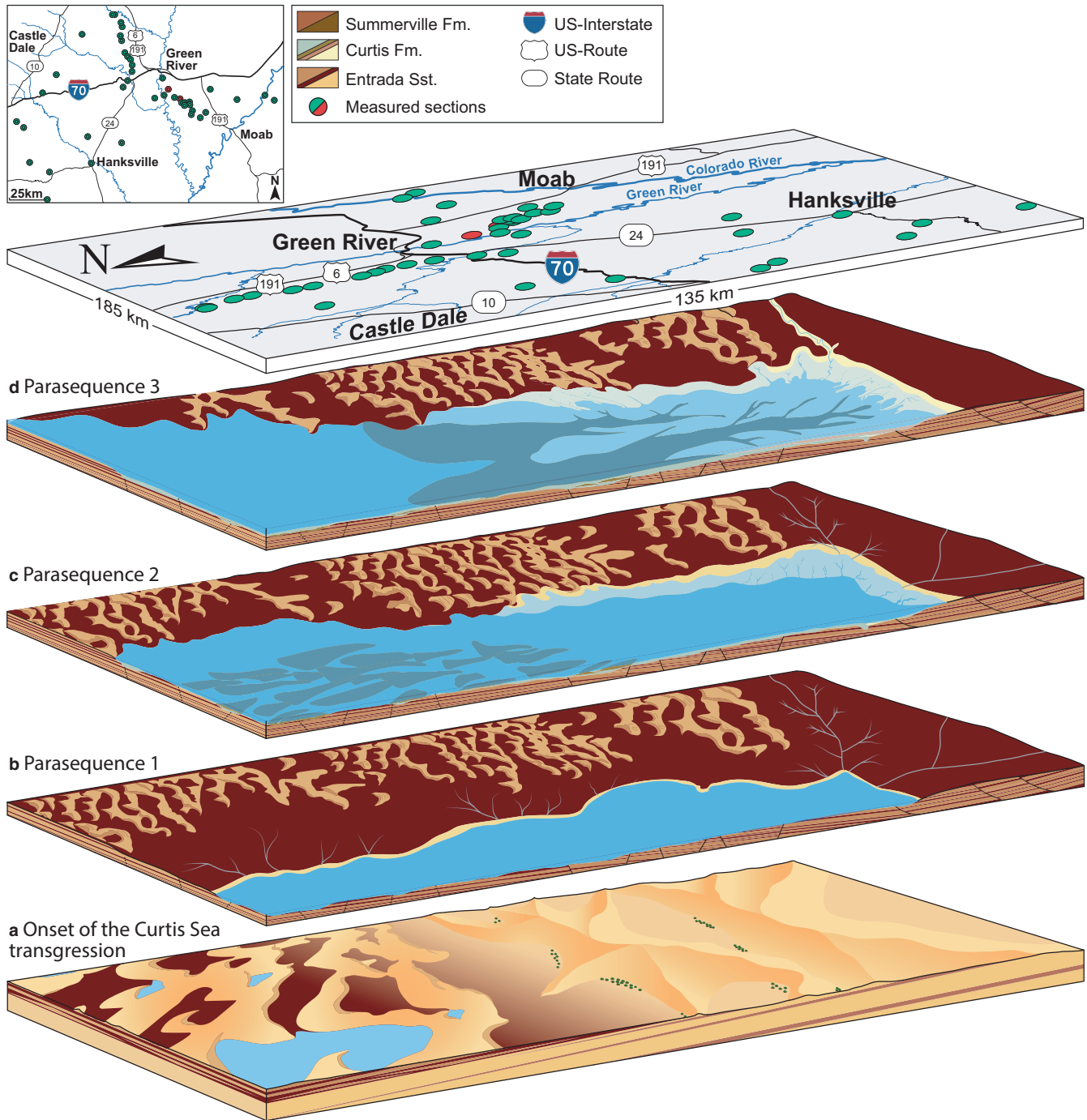
**FIGURE 9** Summary basinal history for the Entrada–Curtis–Summerville interval: (a) As the Curtis Sea transgression had started but had not yet flooded the study area, the paralic deposits of the earthy facies of the Entrada Sandstone developed contemporaneously to the aeolian dunes of the Slick Rock Member of the Entrada Sandstone. (b–d) As the Curtis Sea kept transgressing, the sea experienced allocyclicly-driven relative sea-level variations, leading to the development of three parasequences in the lower Curtis, each bounded by traceable flooding surfaces. (e) The Major Transgression flooded the entire study area (and beyond), and marks the base of the middle Curtis. (f, g) As the Curtis Sea started regressing, the middle Curtis was coexisting with the shallower upper Curtis, the sabkha deposits of the Summerville Formation, and the aeolian dunes of the Moab Member of the Curtis Formation. The development of the paralic domain and coastal dunes was dictated by allocyclically driven relative sea-level variations. The shallow-marine part of the system was under the influence of tidal resonance, leading to the dominance of autocyclic processes, and the overprinting of the relative sea-level signature in the sedimentary record. (h) The Curtis Sea kept regressing, and the sediment supply necessary to the survival of the aeolian dunes of the Moab Member of the Curtis Formation was shut down, and the coastal dune field was terminated, as the entire study area was occupied by the paralic deposits of the Summerville Formation
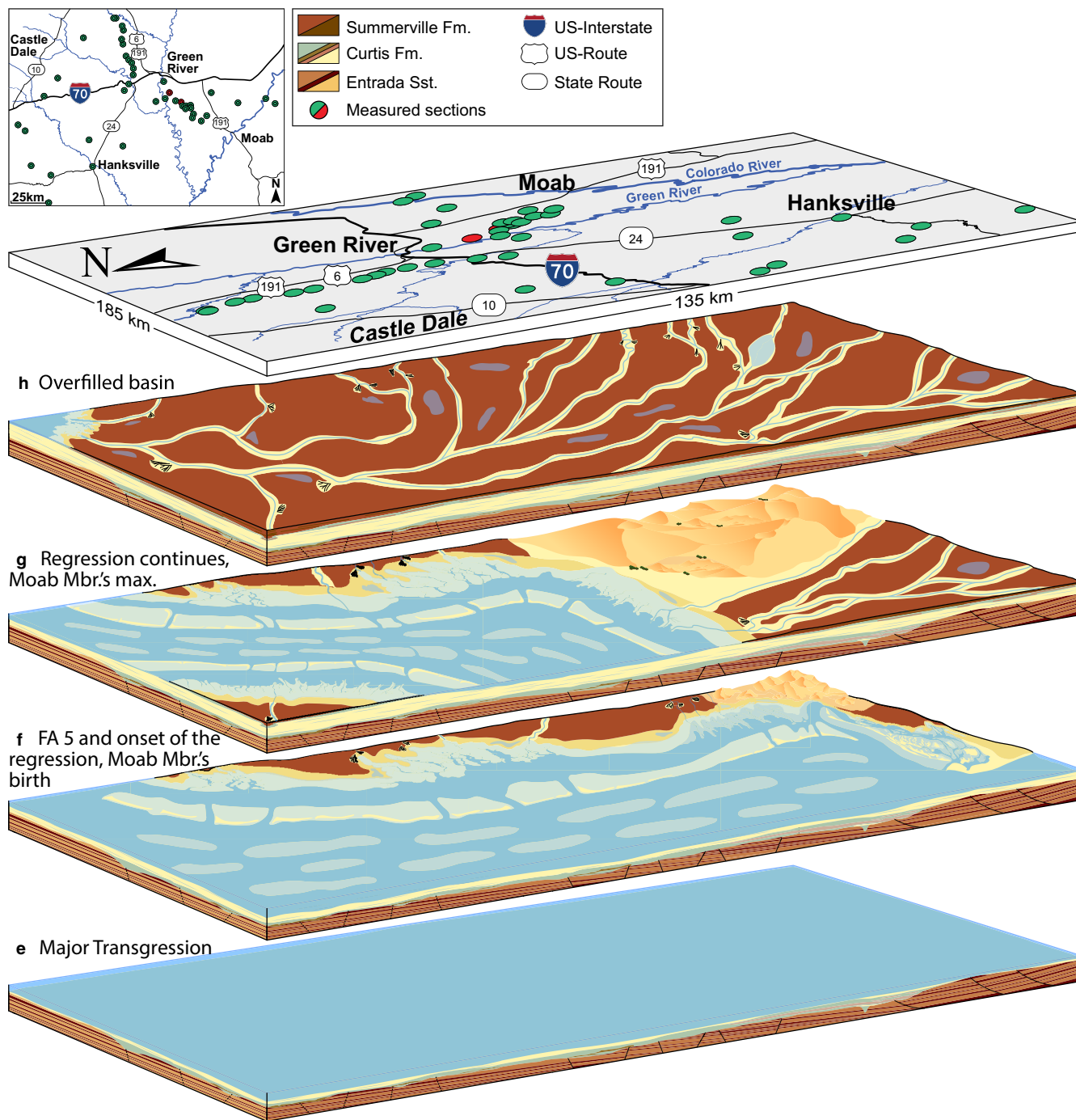
**FIGURE 9** Continued

and grain size with increasing proximity to the coastline are in direct contrast to the classical 'coarse to fine-grained', trend observed within modern-day, tide-dominated environments (Figure 1; Boyd et al., 1992; Dalrymple et al., 1992; Harris et al., 2002; Fan, 2012).

The exclusive occurrence of the gravel-rich dunes and conglomeratic subtidal channels at the localities north of Dry Mesa (6) and Last Chance Desert (38, 39) (Figure 6), may be symptomatic of tidally influenced environments, in which higher energy tidal currents were in operation.

Palaeocurrent indicators from the lower Curtis (Figure 4) and basinward orientation of dune foresets, suggest a strong basin-floor ebb-current over the area (Figure 4b). Each of the three major upward-shallowing successions that characterize the lower Curtis reflects short-lived variations in relative sea level (Figures 4 and 10). Traceable erosive surfaces within the upward-shallowing successions in the more proximal part of the system (Figure 4) are interpreted as regressive surfaces of marine erosion. Each of these surfaces testify to major basinward shifts of the facies belt across the low-gradient Curtis
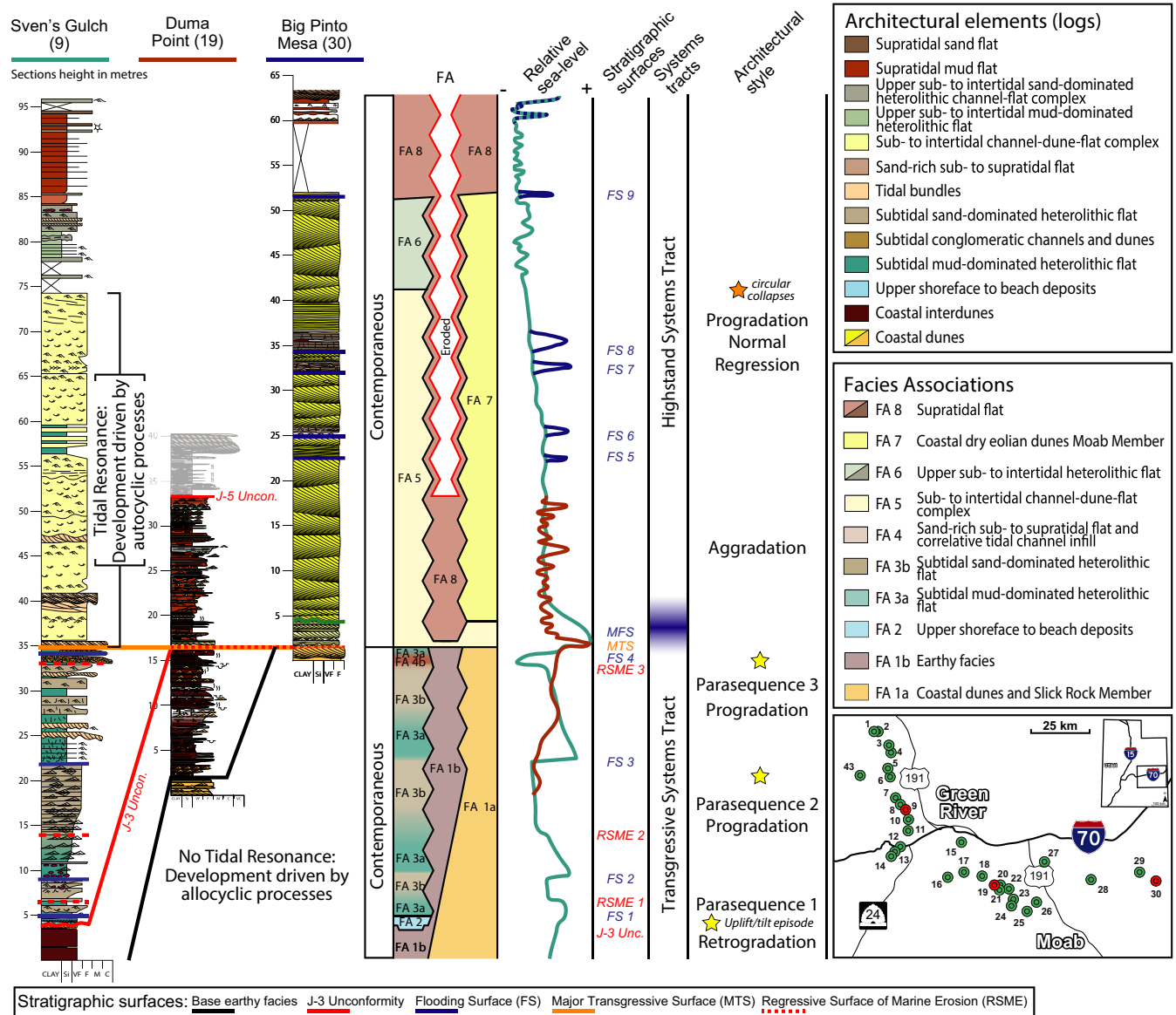
**FIGURE 10** Comparison between the relative sea-level signal recorded by the marine part (Sven's Gulch, left red dot on the map), the paralic neighbouring systems at Duma Point (middle red dot on the map), and the aeolian Moab Member of the Curtis Formation (Big Pinto Mesa, right red dot on the map), illustrating the overwriting of allocyclic signals by the tide-dominated system once it entered in resonance, accompanied by the deposition of the middle Curtis, whereas the contemporaneous aeolian deposits kept recording such allocyclicly forced relative sea-level variations. The paralic succession also shows obvious cyclical floodings, but the accurate relationship between these observed cycles with the neighbouring systems remains puzzling. See Figure 11 for illustration of uplift phases. RSME, Regressive Surface of Marine Erosion; FS, Flooding Surface; MTS, Major Transgressive Surface; MFS, Maximum Flooding Surface; TST, Transgressive System Tract; HST, High Stand System Tract

Sea basin, followed by the deposition of the most proximal and shallowest strata of each upward-shallowing succession. These regressive surfaces of marine erosion are absent from the most distal and basinward part of the system in the north (Figure 4); a consequence of higher slope gradients in the distal areas compared with more proximal parts of the basin. These upward-shallowing successions were subsequently flooded as the relative sea-level rose, and are thus bounded by flooding/ravinement surfaces. Consequently, the three upward-shallowing successions represent parasequences (P1, P2, P3).

The steep incisions (Figure 3e) developed at the top of the lowermost parasequence (P1) are a consequence of a short-lived, decametre-scale fall in relative sea level that accompanied the development of the second parasequence (P2) (Zuchuat et al., 2018, in press). The amplitudes of the relative sea-level variations increase up-section (Figure 10) such that FA4a proximal, subtidal to supratidal sandflat deposits (Figure 3f), and correlative FA 4b gravel-rich, subtidal channels (Figure 3g) prograded basinwards during the uppermost parasequence (P3), as a result of the most pronounced facies belt shift recorded

within the lower Curtis (Figures 4, 9d and 10). However, despite increases in the amplitudes of relative sea-level variations during Curtis times, some of the distal parts of the basin directly adjacent to Cedar Mountain (43) (Figure 11) were less influenced by relative sea-level variations during the development of P3 than their more proximal counterparts, as FA 4b subtidal channels did not reach these distal areas.

## 5.3 | Major transgression

The top of the lower Curtis is capped by the MTS as a consequence of an abrupt relative sea-level rise which completely flooded the study area (Figure 9e), and the area as far south as the present day New Mexico border (Zuchuat et al., 2018, in press). This surface is a complex arrangement of paraconformities and disconformities (Zuchuat et al., 2018, in press). The area between Interstate 70 (12), Shadscale Mesa (13) and Uneva Mine Canyon (14), as well as Cedar Mountain (43) (Figure 11), shows evidence of sub-regional, early Oxfordian uplift prior to the Major Transgression in the lower Oxfordian (Zuchuat et al., 2018, in press), as the MTS truncates lower Curtis strata with an angular relationship.

The sediments of FA 5, particularly subaqueous dunes with associated abundant reactivation surfaces, and sandflats with a strong bidirectional current component (Figures 6i and 7e–h) are in stark contrast to the underlying lower Curtis strata and suggest a higher energy level within the marine system by middle Curtis times (Figures 10 and 12). Grain sizes generally fine toward the coastline and the middle Curtis thickens toward the distal basin (Zuchuat et al., 2018), as is common in many modern-day, tide-dominated environments (Figure 1; Boyd et al., 1992; Dalrymple et al., 1992; Fan, 2012; Harris et al., 2002). The partial flooding of the Slick Rock Member resulted in the reworking of these aeolian dunes sediments into the deposits of the middle Curtis (Figures 4 and 8; Dickinson & Gehrels, 2009, 2010).

A distinctive characteristic of the middle Curtis is the amalgamation of cross-stratified bedforms, coupled with the absence of traceable stratigraphic surfaces (Figures 4 and 10). Such a dramatic shift in sedimentology within an elongated, semi-enclosed basin of this size may be interpreted as the onset of tidal resonance within the Curtis Sea resulting in overprinting of any significant sedimentary response to allocyclic forcing by autocyclic processes (Godin, 1993; Sztanó & de Boer, 1995; Yoshida et al., 2007). Because the system enters tidal resonance, and the signatures of autocyclic processes dominate the sediments, it is impossible to trace a maximum flooding surface (MFS) across localities (Figures 4 and 10). However, upward-thinning, and upward-fining of FA 5 deposits, as well as the overall up-section progradation of the sediments, suggest that a MFS is likely to be located within the lowermost few metres of the middle Curtis (Figure 10).

## 5.4 | Curtis Sea regression

As the Curtis Sea retreated rapidly from the eastern inundated coastal plains, the system saw the concomitant development of a dry aeolian dune system (FA7; Kocurek, 2003; Kocurek & Havholm, 1993; Kocurek & Lancaster, 1999), neighboured by an extensive supratidal flat (FA 8, Figure 10). The calm and restricted setting for FA 6 strata suggests deposition in the proximal and protected zones of the contemporaneous marine system, and FA 5 sediments with metre-scale bedforms were deposited in the distal setting to the west and north (Figures 8, 9f and 12). The asymmetrical, eastward-pinching FA 5 and FA 6 deposits, overlain by FA 8 supratidal sediments, and the growth of the aeolian dune fields of FA 7 (Moab Member; Figures 8 and 9g), suggest rapid coastline progradation, accompanied by increased sediment availability for aeolian transport. As a result, FA 7 thickens eastwards, and its five distinct aeolian packages may be interpreted as sequences (sensu Kocurek, 1988) separated by subtidal to intertidal deposits in its western parts (Figures 8 and 10), and by correlative supratidal deposits, as well as by local development of palaeosol and rhizoliths towards the present day Utah–Colorado border (Zuchuat et al., 2018). These five sequences of the Moab Member likely reflect humid–arid climate variations (Kocurek, 1988; Mountney, 2006, 2012) during which episodes of relative base-level fall promoted growth of the aeolian system, and transgressive phases partially inundated and terminated the aeolian dune field. The abrupt termination of dune fields of FA 7 (Figure 9h) contrasts with the gradual infill of the contemporaneous marine basin by FA 6 and FA 8, suggesting that a major climate shift as an explanation for the termination of the dune fields cannot be justified. It is proposed that a final, short-lived marine transgression shut down the sediment supply to the aeolian system, preserved it in its final form, and deposited a thin interval (<1 m) of shallow-marine deposits to supratidal deposits, with localised sand stromatolite structures.

## 5.5 | The relative influence of autocyclic and allocyclic processes upon the system

Sedimentary and Gamma-ray log data presented here indicate that the Entrada–Curtis–Summerville interval was influenced continuously by allocyclic processes, most notably by relative sea-level variations and climate changes, but also by sub-regional uplift episodes (Figures 5, 8 and 10; Zuchuat et al., in press). The Gamma-ray log data (Figure 8) display cyclical patterns within the studied interval, with no obvious periods of non-deposition or erosion documented in the sedimentology. The marine influence upon the sediments of the earthy facies, together with the ravinement diagnostic of the J-3 Unconformity (Zuchuat et al., in press), suggest near-continuous sedimentation from the earthy facies of the Entrada Sandstone, through lower Curtis

**FIGURE 11** (a) Photogrammetric model of Cedar Mountain showing the earthy facies of the Entrada Sandstone, the erosive relief developed at its top, as well as the lower and middle Curtis strata overlying the J-3 Unconformity. (b, c) Vertically exaggerated interpreted model, which illustrates the impact of both allocyclic and autocyclic forcing on the system as the lower Curtis was developing. Allocyclic forcing: The angular relationship between the different strata indicates that a first tilting of the Entrada Sandstone strata occurred prior to the deposition of Parasequence 1 deposits, a second one occurred before Parasequence 3 developed, and the last one preceded the Major Transgression. Further, the effect of relative sea-level variations, accompanied by the shift of the FAs belt, resulted in the development of the three parasequences. Autocyclic forcing: The minor spatio-temporal energy variations, as well as the WSE-ENE laterally migrating subtidal channel (pink-purplish tones) illustrate best the intrinsically dynamic behaviour of the tide-dominated system, but its multi-storey incision-amalgamation also testifies of a potential impact of external forcing over the system. This contrasts with the middle Curtis' system and its behaviour, which was impacted and developed quasi exclusively as a response of autocyclic forcing

transgressive deposits, into the post-Major-Transgressive middle- and upper Curtis sediments, and associated strata of the Summerville Formation. Consequently, the succession would present an ideal candidate for future work that could analyse relative dominance of allocyclic or autocyclic processes upon sediment dispersal and the preserved strata.

During deposition of the lower Curtis, the system was not in tidal resonance, as the system responded to both autocyclic and allocyclic processes, as observed at Cedar Mountain (43) (Figure 11). The heterogeneous energy distribution of the tidal system was responsive to minor changes in basin morphology, influencing the sediment dispersion and bedform development as part of a self-sustained feedback loop (sensu Cecil, 2003; de Boer, Roos, Hulscher, & Stolk, 2011). Minor current reorganization was probably responsible for local incisions and/or continuous deposition within each of the three parasequences (Figure 10), in contrast to regionally significant and regionally traceable stratigraphic surfaces.

The Major Transgression and the resulting MTS, which defines the base of the middle Curtis, flooded locations beyond the extent of the present study area (Zuchuat et al., 2018, in press), and allowed the system to enter a tidally resonant stage. Traceable stratigraphic surfaces generated by allocyclic relative sea-level variations were not preserved, as autocyclic processes dominated the marine system (Figures 6, 7 and 10). However, retreat of the Curtis Sea was accompanied by the development of the extensive supra-tidal flats of the Summerville Formation (FA 8), and the coastal aeolian systems of the Moab Member of the Curtis Formation (FA 7). Contrary to the dominance of autocyclic process acting upon the deposits of the contemporaneous and resonant tide-dominated system, autocyclic processes impacting on FA 7 and FA 8 were strongly influenced and modulated by allocyclic relative sea-level variations and associated climate oscillations (Figures 8 and 10; Kocurek, 2003; Kocurek & Havholm, 1993; Mountney, 2006).

In addition to modulating the morphology, scale, and type of bedforms occurring within the supratidal and coastal aeolian systems, allocyclic processes were responsible for the rate at which these sediments accumulated and the cyclic arrangement of those sediments. This is visible in the vertical stacking of the aeolian sequences of the Moab Member, which are terminated by marine flooding in the areas close to the palaeo-coastline, whereas palaeosols and superficial vegetation commonly developed where the system remained unflooded by these short-lived marine transgressions.

# 6 | DISCUSSION

The sequence stratigraphic model for the Entrada–Curtis–Summerville interval presented in the study interprets sediments of the Curtis Formation to be deposited in a shallow-marine to marginal-marine setting with variable tidal influence. The lower Curtis sediments (FA2–FA4) represent early marine transgression of the Curtis Sea in which three parasequences can be correlated by the flooding surfaces that bound them. The sedimentary signature of tidal influence is present within the shallowing upwards successions but it is subordinate to the effects of allocyclic controls upon the sedimentology. The middle Curtis sediments (FA5) represent a significantly higher energy environment impacted by tidal processes, but lack both wave-related sedimentary structures and surfaces of sequence-stratigraphic significance. This is interpreted as the overprinting of allocyclic sedimentary signatures by those of a dominant and localized tidal influence. Consequently, the Curtis Sea was in a state of tidal resonance during middle Curtis times. The upper Curtis sediments (FA6–FA8) display stratigraphically significant surfaces that represent marine regression, and the influence of tidal processes upon the sedimentology is subordinate.

It is important to note that similar bedforms to the ones observed in the Curtis Formation (Figure 7) do occur in other depositional systems in which tidal currents act only as a modulating factor rather than a dominant control upon sedimentary character (Baas et al., 2016; Gugliotta, Flint, Hodgson, 2016; Martinius & Gowland, 2011). However, because of the lack of any major fluvial systems within the neighbouring and contemporaneous Entrada Sandstone and Summerville
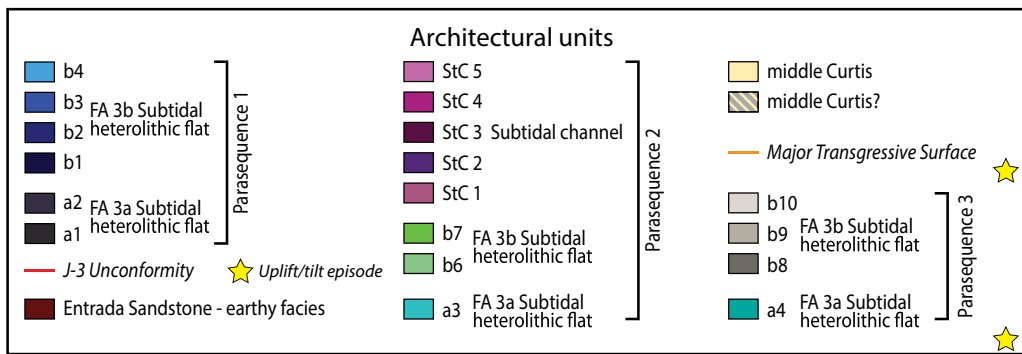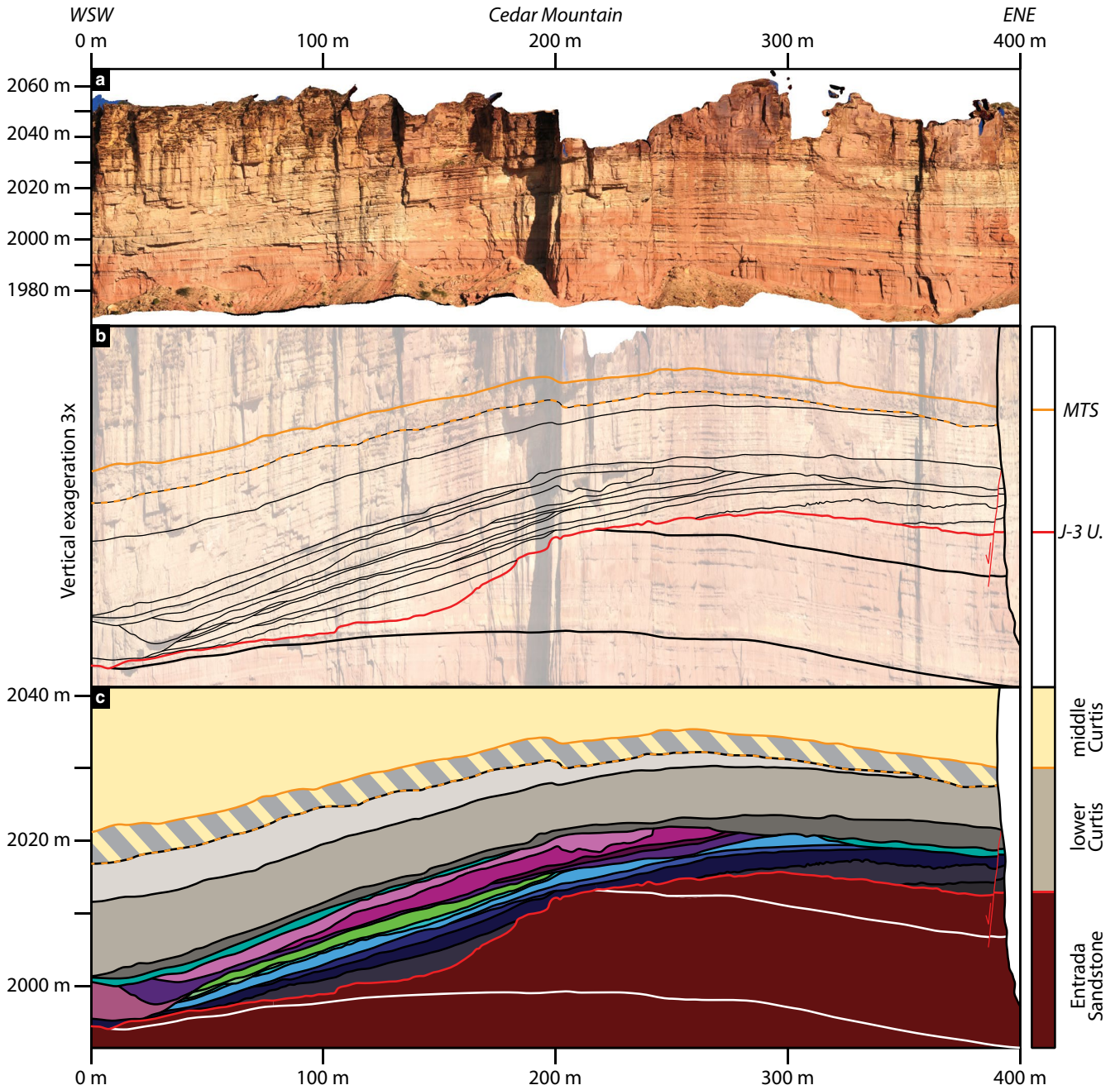
Architectural units

| | | |
|---|---|---|
| b4 | StC 5 | middle Curtis |
| b3 FA 3b Subtidal | StC 4 | middle Curtis? |
| b2 heterolithic flat | StC 3 Subtidal channel | |
| b1 | StC 2 | *Major Transgressive Surface* |
| a2 FA 3a Subtidal | StC 1 | |
| a1 heterolithic flat | | b10 |
| *J-3 Unconformity* | b7 FA 3b Subtidal | b9 FA 3b Subtidal |
| *Uplift/tilt episode* | b6 heterolithic flat | b8 heterolithic flat |
| Entrada Sandstone - earthy facies | a3 FA 3a Subtidal heterolithic flat | a4 FA 3a Subtidal heterolithic flat |

Parasequence 1, Parasequence 2, Parasequence 3

MTS, J-3 U., middle Curtis, lower Curtis, Entrada Sandstone

Vertical exaggeration 3x

**FIGURE 12** Models representing the spatial distribution of the different FA across and idealized Curtis-like basin during the lower Curtis, as well as the middle-upper Curtis intervals, and their correlative energy level's spatial distribution within the system, both before and after the system entered in tidal resonance once the basin threshold dimension was reached. After Sztanó and de Boer (1995), the transgressing Curtis Sea is suggested to have entered at least two other phases of tidal resonance before reaching its maximal extent of *c.* 800 km. Note the coarsening trend from the distal parts of the basin and towards the shoreline in the lower Curtis, with the replacement of the mud-dominated FA 3a deposits, by FA 3b's and FA 4a's coarser-grained and cleaner sediments. Palaeogeographic Map ©2014 Colorado Plateau Geosystems Inc

Formation, as well as the absence of wave current indicators, a hypothesis of a mixed-energy system for Curtis times is difficult to reconcile. The near-exclusively tidally influenced deposits of the Curtis Formation, coupled with a semi-enclosed, elongated basin configuration at the time, suggest the onset of tidal resonance is a reasonable hypothesis for the major energy jump accompanying the deposition of the middle Curtis (Longhitano et al., 2012; Martinius & Gowland, 2011; Reynaud & Dalrymple, 2012; Roos & Schuttelaars, 2011; Shaw et al., 2014; Sztanó & de Boer, 1995).

## 6.1 | Facies distribution, energy levels, basin geometry and tidal resonance

The sedimentology of the Curtis Formation suggests that energy levels within the Curtis Sea during deposition of the lower Curtis sediments were generally lower than those present during deposition of the middle and upper Curtis sediments. However, the distal to proximal sedimentological trends displayed within the lower Curtis are counter to those normally expected within tidally dominated systems (Boyd et al., 1992; Dalrymple et al., 1992; Fan, 2012; Harris et al., 2002). They imply a generally consistent average energy level towards the coast at the time of deposition, compared to a spatial and temporal partitioning of energy levels distally (Figure 12) that promote development of conglomeratic channels and dunes within a finer-grained matrix (Figure 4a). This may be explained by a tidal reworking within a confined basin of extra-basinally sourced flash flood deposits (Zuchuat et al., 2018), that may have originated from the neighbouring, uplifted Uncompahgre Terraces to the east (Otto & Picard, 1976; Scott et al., 2001), and/or from uplifted highlands to the west (Anderson, 2015; Thorman, 2011). Similar gravel to pebble to cobble sized conglomeratic bedforms are found in modern, tidally influenced and confined basins, such as the Bay of Fundy (Li, Shaw, Todd, Kostylev, & Wu, 2014; Shaw et al., 2014; Todd, Shaw, Li, Kostylev, & Wu, 2014), the San Francisco Bay (Barnard, Hanes, Rubin, & Kvitek, 2006) or the bay of Brest (Gregoire, Ehrhold, Le Roy, Jouet, & Garlan, 2016). Alternatively, conglomeritic channels and dunes may result from the influx of a coarser sediment as short-lived regressive pulses brought material from the proximal part of the basin into distal areas, and regressive pulses are notable during the development of the uppermost parasequence P3 (Zuchuat et al., 2018).

The southwards increase in energy, and the presence of sandier and more homogeneous strata within the more proximal parts of the system, may be linked also to tidal amplification as a result of an optimal basin configuration (Godin, 1993; Sztanó & de Boer, 1995; Yoshida et al., 2007) that developed towards the end of lower Curtis times. This may be the pre-cursor to the onset of tidal resonance in middle Curtis times. The physical dimensions of the basin, along with the subdued nature of the pre-transgression relief by this time (Godin, 1993; Sztanó & de Boer, 1995; Yoshida et al., 2007) may serve to promote resonance.

As the dimensions of the semi-enclosed, fluvially starved Curtis Sea reached approximately 800 km in length, and at least 150 km in width, it is possible to determine whether an amphidromic tidal system (Sztanó & de Boer, 1995) could have developed that may provide an explanation for the sedimentology observed. The water depth ($d$) in tidal systems can be determined from the average bedform thickness of the tallest features observed in the succession ($h$) by (Allen, 1968):
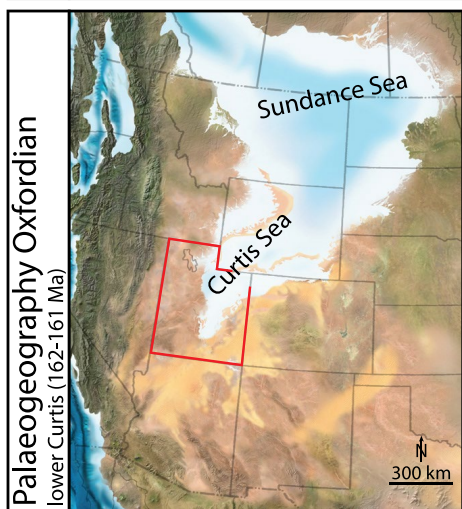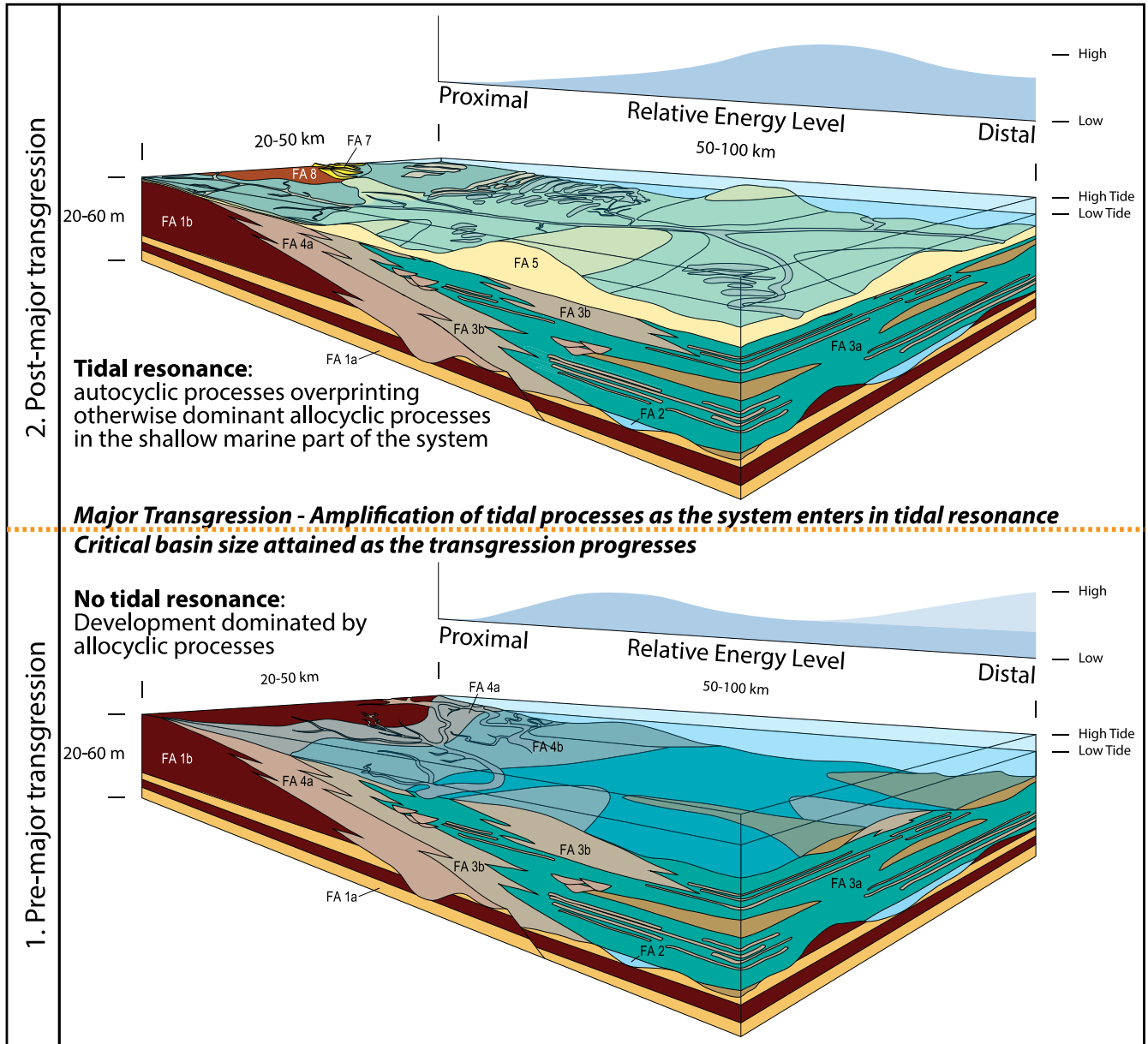
$$h = 0.086 \, (d)^{1.19} \qquad (1)$$

In the Curtis sediments, bedform thickness $h$ can reach 3–4 m, which gives a minimum approximation for the deepest waters of the Curtis Sea in the study area of approximately 20–25 m. The Rossby Deformation Radius ($R$) for a given palaeo-latitude approximately indicates the required basin width for an amphidromic system to develop (Sztanó & de Boer, 1995):
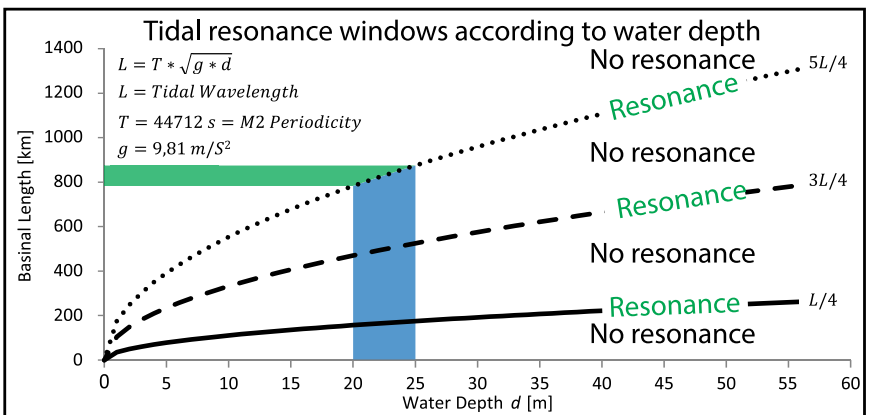
$$R = \sqrt{g \times d}/f \qquad (2)$$

where $g$ is the gravitational acceleration (9.81 m/s²), $d$ the water depth, and $f$ the Coriolis coefficient ($8.3651 \times 10^{-5}$ rad/s at 35° latitude; after Vallis' 2017 Coriolis coefficient equation; palaeolatitude after Hintze and Kowallis 2009). The solution to Equation (2) is approximately 167.5 km, which is close to the width of the Curtis Sea. The calculations imply that an amphidromic system could have developed within the Curtis Sea basin, but the location of the rotational centre of the tidal wave remains unknown and impossible to constrain.

Tidal resonance can develop within a semi-enclosed basin, such as the Gulf of California, the Adriatic Sea, the Persian Gulf, or the Bay of Fundy (Longhitano et al., 2012; Martinius & Gowland, 2011; Reynaud & Dalrymple, 2012; Roos & Schuttelaars, 2011; Shaw et al., 2014; Sztanó & de Boer, 1995), if the length of the embayment approaches an

**2. Post-major transgression**

Proximal

Relative Energy Level

50-100 km

Distal

— High
— Low

20-50 km   FA 7

FA 8

20-60 m   FA 1b

FA 4a

FA 5

FA 3b

FA 3b

FA 3a

FA 1a

FA 2

— High Tide
— Low Tide

**Tidal resonance**:
autocyclic processes overprinting
otherwise dominant allocyclic processes
in the shallow marine part of the system

*Major Transgression - Amplification of tidal processes as the system enters in tidal resonance*
*Critical basin size attained as the transgression progresses*

**No tidal resonance**:
Development dominated by
allocyclic processes

Proximal

Relative Energy Level

50-100 km

Distal

— High
— Low

**1. Pre-major transgression**

20-50 km

FA 4a

FA 4b

20-60 m   FA 1b

FA 4a

FA 3b

FA 3b

FA 3a

FA 1a

FA 2

— High Tide
— Low Tide

**Palaeogeography Oxfordian**
lower Curtis (162-161 Ma)

Sundance Sea

Curtis Sea

300 km

Curtis Sea: ca. 800 km long; **water depth $d$** (Allen, 1968): $h = 0.086(d)^{1.19}$
$h$: average thickness of the tallest bedform, $h = $ 3-4 m; then **$d = $ 20-25 m**

### Tidal resonance windows according to water depth

$L = T * \sqrt{g * d}$
$L = Tidal\ Wavelength$
$T = 44712\ s = M2\ Periodicity$
$g = 9,81\ m/S^2$

No resonance          $5L/4$

Resonance

No resonance          $3L/4$

Resonance

Resonance          $L/4$

No resonance

No resonance

Basinal Length [km]

Water Depth $d$ [m]

odd multiple of a quarter of the tidal wavelength (Godin, 1993; Sztanó & de Boer, 1995; Yoshida et al., 2007):

$$L = T \times \sqrt{g \times d} \qquad (3)$$

where $L$ is the tidal wavelength, $T$ the period of the M2 tide (44′712 s; Roos & Schuttelaars, 2011), $g$ the gravitational acceleration (9.81 m/s$^2$), and $d$ the water depth. However, such resonant behaviour depends also upon the basal shear stresses and the subaqueous morphology of the tidal system (Roos & Schuttelaars, 2011; Wang, Liu, & Lv, 2014).

For water depths $d$ of approximately 20 and 25 m (Equation 1), the tidal wavelength $L$ approaches approximately 625 or 700 km, respectively, which gives a quarter wavelength of approximately 156 or 175 km, respectively. As these values are approximately one-fifth of the total length of the Curtis Sea, tidal resonance could have developed within the basin and may provide some explanation for the variation in sedimentology observed throughout Curtis times.

The phenomenon of resonance may have been triggered by the Major Transgression at the base of the middle Curtis, the regional extent and abrupt nature of which may be linked to an allocyclic, orbitally-forced, relative sea-level rise during the Lower Oxfordian (Boulila et al., 2010, 2011; Pellenard et al., 2014; Strasser et al., 2012). The resultant tidally resonant system, as the middle and upper Curtis were being deposited, was dominated by autocyclic interactions, which overprinted the stratigraphic signatures of most Lower Oxfordian, allocyclic relative sea-level variations (Boulila et al., 2010, 2011; Pellenard et al., 2014; Strasser et al., 2012).

## 6.2 | Causes of cyclcity

Both 405 and 100 ka, orbitally forced eccentricity cycles have been documented within the Tethyan Ocean during the Callovian and Oxfordian ages, within which $\delta^{18}O$ isotopic data indicate a cooling event during the Upper Callovian Age (Boulila et al., 2010, 2011; Pellenard et al., 2014; Strasser et al., 2012). Such a cooling episode, accompanied by increased sediment available for wind transport, may explain the growth and demise of the Entrada aeolian system. Consequently, it may be suggested that sedimentary cycles recorded in the Entrada Sandstone, the lower Curtis, the Moab Member of the Curtis Formation, and the Summerville Formation (Figures 8 and 10), may be related to one (or both) of these two Milankovitch-type cycles. However, the exact nature of relative sea-level variations remains uncertain, and precise dating of the shallow-marine, supratidal, and aeolian deposits of the studied area and their local equivalents would be required in order to determine cycle period

(or frequency). Considering the five aeolian sequences of the Moab Member of the Curtis Formation, each truncated by shallow-marine or superficially vegetated palaeosol horizons, it seems that relative base-level/sea-level oscillations and the arid-humid climate variations were responding simultaneously to the above-mentioned eccentricity cycles.

However, short-lived episodes of sub-regional tectonic uplift have accompanied deposition of parts of the Entrada-lower Curtis interval, which may have impacted upon relative sea level within the basin (Figures 10 and 11; Zuchuat et al., 2018, in press). It seems unlikely that such localized uplift episodes and associated relative sea-level oscillations triggered a simultaneous climate adjustment in the continental, contemporaneous counterparts to the shallow-marine system. Nevertheless, multiple short-lived episodes of tectonic uplift occurred during the deposition of the lower Curtis; the potential climate response of the arid paralic and continental realms to such sub-regional uplift events is difficult to fully assess. Furthermore, debate persists over whether the eccentricity cycles lead to small-scale, glacio–eustatic sea-level variations (Alberti et al., 2012; Chumakov, Zakharov, & Rogov, 2014; Donnadieu et al., 2011; Dromart et al., 2003; Wierzbowski, Dembicz, & Praszkier, 2009), or whether these sea-level variations are due to orbitally forced cycles, of thermal water expansion and/or ground-water recharge (Boulila et al., 2011; Schulz & Schäfer-Neth, 1997).

The amplitude of the relative sea-level variations also remains unconstrained. However, tidal incision at Sven's Gulch (9) (Figure 3e), suggests relative sea-level variations of the order of one decametre. This magnitude matches estimations of the amplitudes of relative sea-level variations within a Mesozoic greenhouse period, driven by 100 or 405 ka eccentricity cycles (Aurell & Bádenas, 2004; Boulila et al., 2010, 2011; Pellenard et al., 2014; Strasser et al., 2012). Consequently, as nine relative sea-level cycles were recorded within the Curtis Formation (Figure 10), it is possible to bracket the time encapsulated within the Curtis Formation to between approximately 0.9 and 3.6 Ma.

## 7 | CONCLUSION

The sediments of the Upper Jurassic Curtis Formation of the Colorado Plateau, Utah, USA, were deposited in a shallow-marine to marginal-marine, tidally dominated environment that responded to allocyclicly controlled fluctuations in relative sea level. Evidence of a strong tidal dominance on deposition includes bi-directional ripple cross-stratified siltstone and sandstone, as well as cross-stratified and heterolithic sandstone with flaser bedding, both of which are often arranged in cyclical tidal bundles. Tidal dominance is

emphasized by a lack of fluvial influence from contemporary and neighbouring systems, and a lack of wave influence within the elongate and shallow basin, propitious to an efficient dissipation of wave energy.

The lower Curtis sediments represent early transgression of the Curtis Sea and are generally contemporaneous with the neighbouring wet interdune to coastal sabkha sediments of the earthy facies of the Entrada sandstone. The lower–middle Curtis boundary represents the onset of major transgression. The middle and upper Curtis units, along with the contemporaneous deposits of the Moab Member of the Curtis Formation and Summerville Formation, represent post-major transgression deposition.

Major stratigraphic surfaces (flooding surfaces, ravinement surfaces, and regressive surfaces of marine erosion) are traceable through sediments of the lower Curtis, and upper Curtis, and their correlative continental equivalents. These surfaces are related to oscillations in relative sea level that may be connected to 100 and or 405 ka Milankovitch cycles, although the exact causes remain equivocal. The surfaces divide the sedimentary succession into a number of packages that are governed by allocyclic process, but display internal sedimentology dominated by tidal processes.

Sediments of the middle Curtis unit are characterized exclusively by tidal facies and a lack of correlatable stratigraphic surfaces. They represent the onset of tidal amplification by resonance within the Curtis Sea. The signatures of allocyclic processes within the sediments are overprinted by those of tidal currents, despite their presence in neighbouring contemporaneous deposits outside of the shallow-marine realm.

The study demonstrates that, given the right sedimentary basin geometry and conditions, the normally dominant allocyclic signatures within shallow-marine sediments related to relative sea-level oscillations may be overprinted and obscured by the usually subordinate localized autocyclic processes of the marine system, such as tides. The importance of examining shallow-marine strata in the context of the deposits of their neighbouring and contemporaneous environments, particularly in settings where the marine basin forms a small and protected embayment, is clear.

## ACKNOWLEDGEMENTS

## CONFLICT OF INTEREST

There are no conflicts of interest in the preparation or publication of this work.

## ORCID

*Valentin Zuchuat* ![iD] https://orcid.org/0000-0002-2029-6422
*Thomas J. H. Dodd* ![iD] https://orcid.org/0000-0003-2257-6740

## REFERENCES

Ahokas, J. M., Nystuen, J. P., & Martinius, A. W. (2014). Depositional dynamics and sequence development in a tide-influenced marginal marine basin: Early Jurassic Neill Klinter Group, Jameson Land Basin, East Greenland. In A. W. Martinius, R. Ravnas, J. Howell, R. J. Steel, & J. Wonham (Eds.), *From depositional systems to sedimentary successions on the Norwegian continental margin*, IAS Special Publication, *46*, 291–338.

Alberti, M., Fürsich, F. T., & Pandey, D. K. (2012). The Oxfordian stable isotope record ($\delta^{18}O$, $\delta^{13}C$) of belemnites, brachiopods, and oysters from the Kachchh Basin (western India) and its potential for palaeoecologic, palaeoclimatic, and palaeogeographic reconstructions. *Palaeogeography, Palaeoclimatology, Palaeoecology*, *344*, 49–68. https://doi.org/10.1016/j.palaeo.2012.05.018

Allen, J. R. L. (1968). The nature and origin of bed-form hierarchies. *Sedimentology*, *10*, 161–182. https://doi.org/10.1111/j.1365-3091.1968.tb01110.x

Anderson, T. H. (2015). Jurassic (170–150 Ma) basins: The tracks of a continental-scale fault, the Mexico-Alaska megashear, from the Gulf of Mexico to Alaska. In T. H. Anderson, A. N. Didenko, C. L. Johnson, A. I. Khanchuk, & J. H. MacDonald (Eds.), *Late Jurassic Margin of Laurasia – A record of faulting accommodating plate rotation*. Geological Society of America Special Papers, *513*, 107–188. https://doi.org/10.1130/9780813725130

Anderson, O. J., & Lucas, S. G. (1994). Middle Jurassic stratigraphy, sedimentation and paleogeography in the southern Colorado Plateau and southern High Plains. In M. V. Caputo, J. A. Peterson, & K. J. Franczyk (Eds.), *Mesozoic systems of the rocky mountain region, USA*. The Rocky Mountain Section SEPM (Society for Sedimentary Geology), Denver, 299–314.

Aurell, M., & Bádenas, B. (2004). Facies and depositional sequence evolution controlled by high-frequency sea-level changes in a shallow-water carbonate ramp (late Kimmeridgian, NE Spain). *Geological Magazine*, *141*, 717–733. https://doi.org/10.1017/S0016756804009963

Baas, J. H., Best, J. L., & Peakall, J. (2016). Predicting bedforms and primary current stratification in cohesive mixtures of mud and sand. *Journal of the Geological Society*, *173*, 12–45. https://doi.org/10.1144/jgs2015-024

Barnard, P. L., Hanes, D. M., Rubin, D. M., & Kvitek, R. G. (2006). Giant sand waves at the mouth of San Francisco Bay. *Eos,*

*Transactions American Geophysical Union*, *87*, 285–289. https://doi.org/10.1029/2006EO290003

Bjerrum, C. J., & Dorsey, R. J. (1995). Tectonic controls on deposition of Middle Jurassic strata in a retroarc foreland basin, Utah-Idaho trough, western interior, United States. *Tectonics*, *14*, 962–978. https://doi.org/10.1029/95TC01448

de Boer, W. P., Roos, P. C., Hulscher, S. J., & Stolk, A. (2011). An idealized model of tidal dynamics in semi-enclosed basins: The effects of a mega-scale sand extraction trench in the North Sea. *Coastal Engineering Proceedings*, *1*, 1–7.

Bonaventura, X., Sima, A. A., Feixas, M., Buckley, S. J., Sbert, M., & Howell, J. A. (2017). Information measures for terrain visualization. *Computers & Geosciences*, *99*, 9–18. https://doi.org/10.1016/j.cageo.2016.10.007

Bostock, J., & Riley, H. T. (1855). *Pliny the elder. The natural history*, 16:1 (2).

Boulila, S., Galbrun, B., Hinnov, L. A., Collin, P. Y., Ogg, J. G., Fortwengler, D., & Marchand, D. (2010). Milankovitch and sub-Milankovitch forcing of the Oxfordian (Late Jurassic) terres noires formation (SE France) and global implications. *Basin Research*, *22*, 717–732. https://doi.org/10.1111/j.1365-2117.2009.00429.x

Boulila, S., Galbrun, B., Miller, K. G., Pekar, S. F., Browning, J. V., Laskar, J., & Wright, J. D. (2011). On the origin of Cenozoic and Mesozoic "third-order" eustatic sequences. *Earth-Science Reviews*, *109*, 94–112. https://doi.org/10.1016/j.earscirev.2011.09.003

Boyd, R., Dalrymple, R., & Zaitlin, B. A. (1992). Classification of clastic coastal depositional environments. *Sedimentary Geology*, *80*, 139–150. https://doi.org/10.1016/0037-0738(92)90037-R

Brenner, R. L., & Peterson, J. A. (1994). Jurassic sedimentary history of the northern portion of the Western Interior Seaway, USA. In M. V. Caputo, J. A. Peterson, & K. J. Franczyk (Eds.), *Mesozoic systems of the rocky mountain Region, USA*. The Rocky Mountain Section SEPM (Society for Sedimentary Geology), Denver, 233–272.

Buckley, S., Ringdal, K., Dolva, B., Naumann, N., & Kurz, T. (2017). LIME: 3D visualisation and interpretation of virtual geoscience models. *EGU General Assembly Conference Abstracts*, *19*, 15952.

Bump, A. P., & Davis, G. H. (2003). Late Cretaceous – early Tertiary Laramide deformation of the northern Colorado Plateau, Utah and Colorado. *Journal of Structural Geology*, *25*, 421–440. https://doi.org/10.1016/S0191-8141(02)00033-0

Burgess, P. M., & Prince, G. D. (2015). Non-unique stratal geometries: Implications for sequence stratigraphic interpretations. *Basin Research*, *27*, 351–365. https://doi.org/10.1111/bre.12082

Caputo, M. V., & Pryor, W. A. (1991). Middle Jurassic tide- and wave-influenced coastal facies and paleography, upper San Rafael Group, east-central Utah. *Utah Geological Association*, *19*, 9–27.

Carr-Crabaugh, M., & Kocurek, G. (1998). Continental sequence stratigraphy of a wet eolian system: A key to relative sea-level change. *Society for Sedimentary Geology, Special Publication*, *59*, 213–228.

Catuneanu, O. (2006). *Principles of sequence stratigraphy*. Amsterdam, The Netherlands: Elsevier, 375 pp.

Catuneanu, O., Abreu, V., Bhattacharya, J. P., Blum, M. D., Dalrymple, R. W., Eriksson, P. G., … Winker, C. (2009). Towards the standardization of sequence stratigraphy. *Earth-Science Reviews*, *92*, 1–33. https://doi.org/10.1016/j.earscirev.2008.10.003

Cecil, C. B. (2003). The concept of autocyclic and allocyclic controls on sedimentation and stratigraphy, emphasizing the climatic variable. In C. B. Cecil, & N. T. Edgar (Eds.), *Climate controls on stratigraphy*. SEPM (Society for Sedimentary Geology) Special Publication, *77*, 13–20. https://doi.org/10.2110/pec.03.77

Chumakov, N. M., Zakharov, V. A., & Rogov, M. A. (2014). Did an ice sheet exist in Northeast Asia at the Middle-Late Jurassic boundary? (Critical remarks on the article by Y. Donnadieu et al. (2011)" A mechanism for brief glacial episodes in the Mesozoic greenhouse"). *Stratigraphy and Geological Correlation*, *22*, 655–658. https://doi.org/10.1134/S0869593814060021

Condon, S. M., & Huffman, A. C, Jr. (1988). Revisions in nomenclature of the middle Jurassic Wanakah Formation, northwestern New Mexico and northeastern Arizona. *U.S. Geological Survey Bulletin*, *1633-A*, A1–A12.

Crabaugh, M., & Kocurek, G. (1993). Entrada sandstone—An example of a wet eolian system. In K. Pye (Ed.), *The dynamics and environmental context of eolian sedimentary systems. London Geological Society Special Publications*, *72*, 103–126.

Dalrymple, R. W., Zaitlin, B. A., & Boyd, R. (1992). Estuarine facies models: Conceptual basis and stratigraphic implications: Perspective. *Journal of Sedimentary Research*, *62*, 1130–1146. https://doi.org/10.1306/D4267A69-2B26-11D7-8648000102C1865D

Dickinson, W. R., & Gehrels, G. E. (2003). U-Pb ages of detrital zircons from Permian and Jurassic eolian sandstones of the Colorado Plateau, USA: Paleogeographic implications. *Sedimentary Geology*, *163*, 29–66. https://doi.org/10.1016/S0037-0738(03)00158-1

Dickinson, W. R., & Gehrels, G. E. (2009). U-Pb ages of detrital zircons in Jurassic eolian and associated sandstones of the Colorado Plateau—evidence for transcontinental dispersal and intraregional recycling of sediment. *Geological Society of America Bulletin*, *121*, 408–433. https://doi.org/10.1130/B26406.1

Dickinson, W. R., & Gehrels, G. E. (2010). Insights into North American paleogeography and paleotectonics from U-Pb ages of detrital zircons in Mesozoic strata of the Colorado Plateau, USA. *International Journal of Earth Sciences*, *99*, 1247–1265. https://doi.org/10.1007/s00531-009-0462-0

Doelling, H. H. (2001). Geologic map of the Moab and eastern part of the San Rafael Desert 30' x 60' quadrangles, Grand and Emery Counties, Utah, and Mesa County, Colorado. Utah Geological Survey Map 180, 3 plates, scale 1:100,000.

Doelling, H. H., Kuehne, P. A., Willis, G. C., & Ehler, J. B. (2015). Geologic map of the San Rafael Desert 30' x 60' quadrangle, Emery and Grand Counties, Utah. Utah Geological Survey, Map 267DM, scale 1:62,500.

Doelling, H. H., Sprinkel, D. A., Kowallis, B. J., & Kuehne, P. A. (2013). Temple Cap and Carmel Formations in the Henry Mountains Basin, Wayne and Garfield Counties, Utah. In T. H. Morris, & R. Ressetar (Eds.), *The San Rafael Swell and Henry Mountains Basin-geologic centerpiece of Utah. Utah Geological Association Publication*, *42*, 279–318.

Donnadieu, Y., Dromart, G., Goddéris, Y., Pucéat, E., Brigaud, B., Dera, G., … Olivier, N. (2011). A mechanism for brief glacial episodes in the Mesozoic greenhouse. *Paleoceanography and Paleoclimatology*, *26*, 1–10.

Dossett, T. S. (2014). The first 40Ar/39Ar ages and tephrochronologic framework for the Jurassic Entrada Sandstone in central Utah. Brigham Young University, Utah, master thesis, 1–46.

Dromart, G., Garcia, J. P., Picard, S., Atrops, F., Lécuyer, C., & Sheppard, S. M. F. (2003). Ice age at the Middle-Late Jurassic transition? *Earth and Planetary Science Letters*, *213*, 205–220. https://doi.org/10.1016/S0012-821X(03)00287-5

Fan, D. (2012). Open-coast tidal flats. In R. A. Davis Jr, & R. W. Dalrymple (Eds.), *Principles of tidal sedimentology* (pp. 187–229). Dordrecht, The Netherlands: Springer Science and Business Media. https://doi.org/10.1007/978-94-007-0123-6

Fertl, W. H., Chilingarian, G. V., & Yen, T. F. (1982). Use of natural gamma ray spectral logging in evaluation of clay minerals. *Energy Sources*, 6(4), 335–360. https://doi.org/10.1080/00908318208946036

Getty, P. R., & Hagadorn, J. W. (2009). Palaeobiology of the Climactichnites tracemaker. *Palaeontology*, *52*, 753–778. https://doi.org/10.1111/j.1475-4983.2009.00875.x

Gilluly, J., & Reeside, J. B, Jr. (1928). Sedimentary rocks of the San Rafael Swell and some adjacent areas in eastern Utah. U.S. Geological Survey, Professional Paper, 150-D, 61–110.

Godin, G. (1993). On tidal resonance. *Continental Shelf Research*, *13*, 89–107. https://doi.org/10.1016/0278-4343(93)90037-X

Gregoire, G., Ehrhold, A., Le Roy, P., Jouet, G., & Garlan, T. (2016). Modern morpho-sedimentological patterns in a tide-dominated estuary system: The Bay of Brest (west Britanny, France). *Journal of Maps*, *12*, 1152–1159. https://doi.org/10.1080/17445647.2016.1139514

Gugliotta, M., Flint, S. S., Hodgson, D. M., & Veiga, G. D. (2016). Recognition criteria, characteristics and implications of the fluvial to marine transition zone in ancient deltaic deposits (Lajas Formation, Argentina). *Sedimentology*, *63*, 1971–2001. https://doi.org/10.1111/sed.12291

Halland, E. K., Bjørnestad, A., Magnus, C., Riis, F., Meling, I. M., Tørneng Gjeldvik, I., … Pham, V. T. H. (2014). *CO2 storage atlas—Norwegian continental shelf*. Stavanger, Norway: Norwegian Petroleum Directorate.

Haq, B. U., Hardenbol, J., & Vail, P. R. (1987). Chronology of fluctuating sea levels since the Triassic. *Science*, *235*, 1156–1167. https://doi.org/10.1126/science.235.4793.1156

Harris, P. T., Heap, A. D., Bryce, S. M., Porter-Smith, R., Ryan, D. A., & Heggie, D. T. (2002). Classification of Australian clastic coastal depositional environments based upon a quantitative analysis of wave, tidal, and river power. *Journal of Sedimentary Research*, *72*, 858–870. https://doi.org/10.1306/040902720858

Heyman, O. (1983). Distribution and structural geometry of faults and folds along the northwestern Uncompahgre Uplift, western Colorado and eastern Utah. In W. Averett (Ed.), *Northern paradox basin-uncompahgre uplift* (pp. 45–57). Grand Junction, CO: Grand Junction Geological Society.

Hintze, L. F. (1980). *Geologic map of Utah*. Utah Geological and Mineral Survey, scale 1:250,000, 2 sheets.

Hintze, L. F., & Kowallis, B. J. (2009). *Geologic history of Utah*. Provo: Utah, Brigham Young University Studies, 225 pp.

Imlay, R. W. (1947). Marine Jurassic of Black Hills Area, South Dakota and Wyoming. *American Association of Petroleum Geologists Bulletin*, *31*, 227–273.

Imlay, R. W. (1952). Marine origin of Preuss sandstone of Idaho, Wyoming, and Utah. *American Association of Petroleum Geologists Bulletin*, *36*, 1735–1753.

Imlay, R. W. (1980). Jurassic paleobiogeography of the conterminous United States in its continental setting. *U.S. Geological Survey Professional Paper*, *1062*, 1–134.

Kocurek, G. (1988). First-order and super bounding surfaces in eolian sequences—bounding surfaces revisited. *Sedimentary Geology*, *56*, 193–206. https://doi.org/10.1016/0037-0738(88)90054-1

Kocurek, G. (2003). Limits on extreme eolian systems: Shara of Mauritania and Jurassic Navajo Sandstone examples. In M. A. Chan, & A. W. Archer (Eds.), *Extreme depositional environments: Mega end members in geologic time*. Geological Society of America Special Paper, *370*, 43–52.

Kocurek, G., & Havholm, K. G. (1993). Eolian sequence stratigraphy: A conceptual framework. In P. Weimer, & H. W. Posamentier (Eds.), *Siliciclastic sequence stratigraphy: Recent developments and applications*. American Association of Petroleum Geologists Memoir, *58*, 393–410.

Kocurek, G., & Lancaster, N. (1999). Aeolian system sediment state: Theory and Mojave Desert Kelso dune field example. *Sedimentology*, *46*, 505–515. https://doi.org/10.1046/j.1365-3091.1999.00227.x

Kocurek, G., Martindale, R. C., Day, M., Goudge, T. A., Kerans, C., Hassenruck-Gudipati, H. J., … Nazworth, C. M. (2018). Antecedent aeolian dune topographic control on carbonate and evaporite facies: Middle Jurassic Todilto Member, Wanakah Formation, Ghost Ranch, New Mexico, USA. *Sedimentology*, 1–30.

Kreisa, R. D., & Moiola, R. J. (1986). Sigmoidal tidal bundles and other tide-generated sedimentary structures of the Curtis Formation, Utah. *Geological Society of America Bulletin*, *97*, 381–387. https://doi.org/10.1130/0016-7606(1986)97&lt;381:STBAOT&gt;2.0.CO;2

Kvale, E. P. (2012). Tidal constituents of modern and ancient tidal rhythmites: Criteria for recognition and analyses. In R. A. Davis Jr & R. W. Dalrymple (Eds.), *Principles of tidal sedimentology* (pp. 1–17). Dordrecht, Netherlands: Springer Science and Business Media.

Levander, A., Schmandt, B., Miller, M. S., Liu, K., Karlstrom, K. E., Crow, R. S., … Humphreys, E. D. (2011). Continuing Colorado plateau uplift by delamination-style convective lithospheric downwelling. *Nature*, *472*, 461–465. https://doi.org/10.1038/nature10001

Li, M. Z., Shaw, J., Todd, B. J., Kostylev, V. E., & Wu, Y. (2014). Sediment transport and development of banner banks and sandwaves in an extreme tidal system: Upper Bay of Fundy, Canada. *Continental Shelf Research*, *83*, 86–107. https://doi.org/10.1016/j.csr.2013.08.007

Longhitano, S. G., Mellere, D., Steel, R. J., & Ainsworth, R. B. (2012). Tidal depositional systems in the rock record: A review and new insights. *Sedimentary Geology*, *279*, 2–22. https://doi.org/10.1016/j.sedgeo.2012.03.024

Lucas, S. G. (2014). Lithostratigraphy of the Jurassic San Rafael Group from Bluff to the Abajo Mountains, southeastern Utah: Stratigraphic relationships of the Bluff Sandstone. *Volumina Jurassica*, *12*, 55–68.

Mansfield, G. R., & Roundy, P. V. (1916). Revision of the Beckwith and Bear River Formations of southeastern Idaho. *U.S. Geological Survey Professional Paper*, *98*, 75–84.

Martinius, A. W., & Gowland, S. (2011). Tide-influenced fluvial bedforms and tidal bore deposits (late Jurassic Lourinhã Formation, Lusitanian Basin, Western Portugal). *Sedimentology*, *58*, 285–324. https://doi.org/10.1111/j.1365-3091.2010.01185.x

Martinius, A. W., Ringrose, P. S., Brostrøm, C., Elfenbein, C., Næss, A., & Ringås, J. E. (2005). Reservoir challenges of heterolithic tidal sandstone reservoirs in the Halten Terrace, mid-Norway. *Petroleum Geoscience*, *11*, 3–16. https://doi.org/10.1144/1354-079304-629

McMullen, S. K., Holland, S. M., & O'Keefe, F. R. (2014). The occurrence of vertebrate and invertebrate fossils in a sequence stratigraphic context: The Jurassic Sundance Formation, Bighorn Basin, Wyoming, USA. *Palaios*, *29*, 277–294. https://doi.org/10.2110/pal.2013.132

Midtkandal, I., & Nystuen, J. P. (2009). Depositional architecture of a low-gradient ramp shelf in an epicontinental sea: The lower

Cretaceous of Svalbard. *Basin Research*, *21*, 655–675. https://doi.org/10.1111/j.1365-2117.2009.00399.x

Mitchum, R. J., Vail, P. R., & Thompson, S., III. (1977). The depositional sequence as a basic unit for stratigraphic analysis. In C. E. Payton (ed.), *Seismic stratigraphy: Applications to hydrocarbon exploration. American Association of Petroleum Geologists Memoir*, *26*, 205–212.

Mountney, N. P. (2006). Periodic accumulation and destruction of aeolian erg sequences in the Permian Cedar Mesa Sandstone, White Canyon, southern Utah, USA. *Sedimentology*, *53*, 789–823. https://doi.org/10.1111/j.1365-3091.2006.00793.x

Mountney, N. P. (2012). A stratigraphic model to account for complexity in aeolian dune and interdune successions. *Sedimentology*, *59*, 964–989. https://doi.org/10.1111/j.1365-3091.2011.01287.x

Murray, K. E., Reiners, P. W., & Thomson, S. N. (2016). Rapid Pliocene-Pleistocene erosion of the central Colorado Plateau documented by apatite thermochronology from the Henry Mountains. *Geology*, *44*, 483–486. https://doi.org/10.1130/G37733.1

Nelson, S. T. (1997). Reevaluation of the Central Colorado plateau laccoliths in the light of new age determination. *U.S. Geological Survey Bulletin*, *2158*, 37–39.

Ogg, J. G., Ogg, G., & Gradstein, F. M.. (2016). *A concise geologic time scale: 2016*. Boston: Elsevier.

Osleger, D. (1991). Subtidal carbonate cycles: Implications for allocyclic vs. autocyclic controls. *Geology*, *19*, 917–920. https://doi.org/10.1130/0091-7613(1991)019&lt;0917:SCCIFA&gt;2.3.CO;2

Otto, E. P., & Picard, M. D. (1976). Petrology of the Entrada Sandstone (Jurassic), northeastern Utah. In J. G. Hill (Ed.), *Geology of the Cordilleran hingeline. Rocky Mountain association of petroleum geologists guidebook*. Denver, Colorado, Rocky Mountain Association of Geologists, p. 231–246.

Pellenard, P., Tramoy, R., Pucéat, E., Huret, E., Martinez, M., Bruneau, L., & Thierry, J. (2014). Carbon cycle and sea-water palaeotemperature evolution at the Middle-Late Jurassic transition, eastern Paris Basin (France). *Marine and Petroleum Geology*, *53*, 30–43. https://doi.org/10.1016/j.marpetgeo.2013.07.002

Peterson, F. (1994). Sand dunes, sabkhas, streams, and shallow seas: Jurassic paleography in the southern part of the Western Interior Basin. In M. V. Caputo, J. A. Peterson, & K. J. Franczyk (Eds.), *Mesozoic systems of the rocky mountain region, USA*. The Rocky Mountain Section SEPM (Society for Sedimentary Geology), Denver, 233–272.

Peterson, F., & Pipiringos, G. N. (1979). Stratigraphic relations of the Navajo Sandstone to Middle Jurassic formations, southern Utah and northern Arizona. *U.S. Geological Survey Professional Paper*, *1035-B*, 1-43.

Pipiringos, G. N., & Imlay, R. W. (1979). Lithology and subdivisions of the Jurassic Stump Formation in southeastern Idaho and adjoining areas. *U.S. Geological Survey Professional Paper*, *1035-C*, 1–25.

Pipiringos, G. N., & O'Sullivan, R. B. (1978). Principal unconformities in Triassic and Jurassic rocks, western interior United States: A preliminary survey. *U.S. Geological Survey, Professional Paper*, *1035-A*, 1–29.

Reynaud, J. Y., & Dalrymple, R. W. (2012). Shallow-marine tidal deposits. In R. A. Davis Jr, & R. W. Dalrymple (Eds.), *Principles of tidal sedimentology* (pp. 335–369). Dordrecht, The Netherlands: Springer Science and Business Media. https://doi.org/10.1007/978-94-007-0123-6

Roos, P. C., & Schuttelaars, H. M. (2011). Influence of topography on tide propagation and amplification in semi-enclosed basins. *Ocean Dynamics*, *61*, 21–38. https://doi.org/10.1007/s10236-010-0340-0

Schulz, M., & Schäfer-Neth, C. (1997). Translating Milankovitch climate forcing into eustatic fluctuations via thermal deep water expansion: A conceptual link. *Terra Nova*, *9*, 228–231. https://doi.org/10.1111/j.1365-3121.1997.tb00018.x

Scott, R. B., Harding, A. E., Hood, W. C., Cole, R. D., Livaccari, R. F., Johnson, J. B., … Dickerson, R. P. (2001). Geologic map of Colorado National Monument and adjacent areas, Mesa County, Colorado. U.S. Geological Map I-2740, 40 pp., 1 plate, scale 1:24,000.

Shaw, J., Todd, B. J., & Li, M. Z. (2014). Geologic insights from multibeam bathymetry and seascape maps of the Bay of Fundy, Canada. *Continental Shelf Research*, *83*, 53–63. https://doi.org/10.1016/j.csr.2013.12.015

Sprinkel, D. A., Doelling, H. H., Kowallis, B. J., Waanders, G., & Kuehne, P. A. (2011a). Early results of a study of Middle Jurassic strata in the Sevier fold and thrust belt, Utah. In D. A. Sprinkel, W. A. Yonkee, & T. C. Chidsey. (Eds.), *Sevier thrust belt: Northern and Central Utah and adjacent areas. Utah Geological Association, Publication*, *40*, 151–172.

Sprinkel, D. A., Kowallis, B. J., & Jensen, P. H. (2011b). Correlation and age of the Nugget Sandstone and Glen Canyon Group, Utah. In D. A. Sprinkel, W. A. Yonkee, & T. C. Chidsey (Eds.), *Sevier thrust belt: Northern and Central Utah and adjacent. Areas Utah Geological Association Publication*, *40*, 131–149.

Strasser, A., Pittet, B., Hillgärtner, H., & Pasquier, J. B. (1999). Depositional sequences in shallow carbonate-dominated sedimentary systems: Concepts for a high-resolution analysis. *Sedimentary Geology*, *128*, 201–221. https://doi.org/10.1016/S0037-0738(99)00070-6

Strasser, A., Vedrine, S., & Stienne, N. (2012). Rate and synchronicity of environmental changes on a shallow carbonate platform (Late Oxfordian, Swiss Jura Mountains). *Sedimentology*, *59*, 185–211. https://doi.org/10.1111/j.1365-3091.2011.01236.x

Sullivan, K. R., Kowallis, B. J., & Mehnert, H. H. (1991). Isotopic ages of igneous intrusions in southeastern Utah – Evidence for a mid-Cenozoic Reno-San Juan magmatic zone. *Brigham Young University Geology Studies*, *37*, 139–144.

Svendsen, J. B., & Hartley, N. R. (2001). Comparison between outcrop-spectral gamma ray logging and whole rock geochemistry: Implications for quantitative reservoir characterisation in continental sequences. *Marine and Petroleum Geology*, *18*, 657–670. https://doi.org/10.1016/S0264-8172(01)00022-8

Sztanó, O., & de Boer, P. L. (1995). Basin dimensions and morphology as controls on amplification of tidal motions (the Early Miocene North Hungarian Bay). *Sedimentology*, *42*, 665–682. https://doi.org/10.1111/j.1365-3091.1995.tb00399.x

Tape, C. H., Cowan, C. A., & Runkel, A. C. (2003). Tidal-bundle sequences in the Jordan Sandstone (Upper Cambrian), southeastern Minnesota, USA: Evidence for tides along inboard shorelines of the Sauk epicontinental sea. *Journal of Sedimentary Research*, *73*, 354–366. https://doi.org/10.1306/091602730354

Thorman, C. H. (2011). The Elko orogeny – A major tectonic event in eastern Nevada–western Utah. In D. A. Sprinkel, W. A. Yonkee, & T. C. Chidsey (Eds.), *Sevier thrust belt: Northern and Central Utah and adjacent areas. Utah Geological Association Publication*, *40*, 117–129.

Todd, B. J., Shaw, J., Li, M. Z., Kostylev, V. E., & Wu, Y. (2014). Distribution of subtidal sedimentary bedforms in a macrotidal setting: The Bay of Fundy, Atlantic Canada. *Continental Shelf Research*, *83*, 64–85. https://doi.org/10.1016/j.csr.2013.11.017

Trudgill, B. D. (2011). Evolution of salt structures in the northern Paradox Basin: Controls on evaporite deposition, salt wall growth

and supra-salt stratigraphic architecture. *Basin Research*, *23*, 208–238. https://doi.org/10.1111/j.1365-2117.2010.00478.x

Valenza, J. M. (2016). Redbeds of the Upper Entrada Sandstone, Central Utah: Facies Analysis and Regional Implications of Interfingered Sabkha and Fluvial Terminal Splay Sediments. Brigham Young University, Utah, Master Thesis, 1–54.

Vallis, G. K. (2017). *Atmospheric and oceanic fluid dynamics*. Cambridge, UK: Cambridge University Press, 745 pp. https://doi.org/10.1017/9781107588417

Walker, R. G. (1992). Facies, facies models and modern stratigraphic concepts. In R. G. Walker & N. P. James (Eds.), *Facies models: Response to sea-level change. Geological Association of Canada*, Toronto, 1–14.

Wang, P. (2012). Principles of sediment transport applicable in tidal environments. In R. A. Davis Jr & R. W. Dalrymple (Eds.), *Principles of tidal sedimentology* (pp. 19–34). Dordrecht, The Netherlands: Springer Science and Business Media. https://doi.org/10.1007/978-94-007-0123-6

Wang, D., Liu, Q., & Lv, X. (2014). A study on bottom friction coefficient in the Bohai, Yellow, and East China Sea. *Mathematical Problems in Engineering*, *2014*, 1–7.

Westoby, M. J., Brasington, J., Glasser, N. F., Hambrey, M. J., & Reynolds, J. M. (2012). 'Structure-from-Motion'photogrammetry: A low-cost, effective tool for geoscience applications. *Geomorphology*, *179*, 300–314. https://doi.org/10.1016/j.geomorph.2012.08.021

Wierzbowski, H., Dembicz, K., & Praszkier, T. (2009). Oxygen and carbon isotope composition of Callovian-Lower Oxfordian (Middle–Upper Jurassic) belemnite rostra from central Poland: A record of a Late Callovian global sea-level rise? *Palaeogeography, Palaeoclimatology, Palaeoecology*, *283*, 182–194. https://doi.org/10.1016/j.palaeo.2009.09.020

Wilcox, W. T., & Currie, B. (2008). Sequence Stratigraphy of the Jurassic Curtis, Summerville, and Stump Formations, Eastern Utah and Northwest Colorado. In M. W. Longman & C. D. Morgan (Eds.), *Hydrocarbon systems and production in the Uinta Basin, Utah.*

*Rocky Mountain Association of Geologists and Utah Geological Association Publication*, *37*, 9–41.

Witkind, I. J. (1988). Geologic map of the Huntington 30' X 60' quadrangle, Carbon, Emery, Grand, and Uintah Counties, Utah. U.S. Geological Survey, Miscellaneous Investigations Series Map I-1764, scale 1:100,000.

Yonkee, W. A., & Weil, A. B. (2015). Tectonic evolution of the Sevier and Laramide belts within the North American Cordillera orogenic system. *Earth-Science Reviews*, *150*, 531–593. https://doi.org/10.1016/j.earscirev.2015.08.001

Yoshida, S., Steel, R. J., & Dalrymple, R. W. (2007). Changes in depositional processes—An ingredient in a new generation of sequence-stratigraphic models. *Journal of Sedimentary Research*, *77*, 447–460. https://doi.org/10.2110/jsr.2007.048

Zuchuat, V., Midtkandal, I., Poyatos-Moré, M., da Costa, S., Brooks, H.L., Halvorsen, K., Cote, N., Sundal, A. & Braathen, A. (in press). Composite unconformities in low-gradient transitional settings: The J-3 unconformity and the curtis formation, East-Central Utah, USA. *The Journal of Sedimentary Research.*

Zuchuat, V., Sleveland, A. R. N., Sprinkel, D. A., Rimkus, A., Braathen, A., & Midtkandal, I. (2018). New insights on the impact of tidal currents on a low-gradient, semi-enclosed, epicontinental basin—The Curtis Formation, east-central Utah, USA. *Geology of the Intermountain West*, *5*, 131–165. https://doi.org/10.31711/giw.v5i0.24